LUND UNIVERSITY

LTH

FACULTY OF ENGINEERING

Automatic Mitral and Tricuspid Valve Flow Quantification using Valve Tracking in 4D Flow MRI

Master's Thesis in Biomedical Engineering

Elisabeth Dierschke Passikhani

Julia Nilsson

June 2026

Supervisor: Einar Heiberg, Medviso
Supervisor: Martin Stridh, Department of Biomedical Engineering
Examiner: Magnus Cinthio, Department of Biomedical Engineering

Medviso AB
Department of Biomedical Engineering
Faculty of Engineering LTH

Abstract

In this project a tool for valve flow quantification from 4D flow data for the mitral and tricuspid valves was developed and integrated into the clinical image analysis software Segment. The pre-implemented neural networks MVnet and TVnet were used for tracking the valves in 2CH and 4CH cine MRI images. The positions of the valves were used to create planes in the 4D flow data to measure flow over one cardiac cycle. An algorithm was created to automatically segment valve flow in these planes where flow from other vessels, such as the aorta, is removed while still including potential backflow in the valve. The automatic tracking performed well in adults, but showed reduced performance for the tricuspid valve in some pediatric cases where tracking failures were observed. The automatic segmentation performed well overall with manual correction required in only 5/44 mitral and 7/42 tricuspid cases. The run time in Segment is around 10-15 seconds which provides a short analysis time compared to a solution with a less automated workflow.

The implemented mitral and tricuspid valve flow quantification methods were validated on datasets comprising different pathological groups acquired on Siemens (n=37) and Philips (n=7) scanners. In the validation the mitral volume corresponding to the flow through the valve during one cardiac cycle was compared with both 4D and 2D aortic measurements. The tricuspid volume was compared with 4D and 2D pulmonary artery measurements. The validation demonstrated strong correlations and low biases but revealed unexpectedly large variability between all volume measurements, making validation challenging. Comparisons with another established valve tracking tool in 4D flow showed largely comparable results.

Encouraging performance was demonstrated, however further investigation and evaluation of the implemented valve flow quantification methods are needed due to remaining variability.

Acknowledgments

We would like to sincerely thank our supervisor Einar Heiberg for all the guidance and support throughout this project. Having someone with such extensive knowledge who has always been readily available for questions and advice has been invaluable. We would also like to extend our gratitude to the whole team at Medviso for providing us with such a supportive and welcoming environment and for always offering help when needed. A special thanks to Fanny Månefjord for always making time to help us with both practical and technical aspects of the project and to Helen Fransson for her guidance and help during the validation process. We are also grateful to the whole cardiac MR-group for all of their support and feedback. Lastly we also thank our fellow students Axel Jensen, Fredrik Hasselberg and Disa Fornell for their support och helpful discussions.

Use of Artificial Intelligence tools

In this project AI was used for improving structure of sentences for the report and discussing theoretical concepts to aid understanding. It was not used to generate sections of texts or used as a sole source of information. In the development of the code, AI was used for understanding and debugging code and making fixes, as well as to search for and compare functions in Matlab when web searches did not provide the needed information. Independent judgement was exercised for all use of AI.

Contents

1

List of Abbreviations

2CH	Two Chamber View
3CH	Three Chamber View
4CH	Four Chamber View
AV	Atrioventricular
ECG	Electrocardiogram
CMR	Cardiovascular Magnetic Resonance
CNN	Convolutional Neural Network
EDT	End diastolic time
EST	End systolic time
MRI	Magnetic Resonance Imaging
MV	Mitral valve
PC-MRI	Phase Contrast Magnetic Resonance Imaging
ROI	Region of interest
TV	Tricuspid valve
VENC	Velocity encoding

2

Introduction

The heart, which is responsible for pumping blood throughout the body, is divided into four chambers. The mitral valve separates the chambers on the left side of the heart, and the tricuspid valve separates the right chambers. The anatomy, function and flow of valves are investigated during assessment and diagnosis of valvular diseases. Currently the most commonly used imaging modality is transthoracic echocardiography. A transthoracic echocardiogram works well for assessment and localization of valvular diseases. By combining this technique with a Doppler the flow through the valves can be measured. Echocardiography is an easy accessible, safe and portable imaging technique.

Magnetic resonance imaging (MRI) is an imaging modality used in cases where the results from the transthoracic echocardiogram are not sufficient for diagnosis. Cardiovascular magnetic resonance (CMR) is a specialized MRI technique adapted for the heart and cardiovascular system where MR images are acquired and reconstructed to create a dynamic image sequence of the cardiac cycle. CMR can offer a more accurate quantification of valvular flow and regurgitation [1]. In 4D flow CMR imaging, three-dimensional MR images with velocity measurements of the whole heart are captured over the duration of several heartbeats from which one cardiac cycle is then reconstructed. The advantage of 4D flow is that flow can be measured in any region of interest within the imaging volume after acquisition, while for 2D images the data is restricted to the chosen plane during imaging.

During the cardiac cycle the mitral and tricuspid valves, in addition to opening and closing, also move up and down with the heart muscle. Retrospective valve tracking enables analysis of valve motion after image acquisition. By identifying valve positions across a 2D MR image sequence covering a full cardiac cycle, their movement can be assessed. This process may be performed manually or automated using AI-based methods. Valve tracking can be combined with 4D flow CMR imaging to measure and quantify flow and regurgitation through the valves.

Medviso AB is a company developing software for visualization and analysis of medical images. One of their developed software is Segment, which is software for quantitative cardiac MRI analysis. Segment CMR is used clinically and has some of the functions of Segment. Segment and Segment CMR have a module for 4D flow analysis where a tool for valve tracking and valve flow analysis was implemented.

2.1 Purpose and Objectives

The purpose of this project was to develop a tool for automatic flow quantification of the mitral and tricuspid valves in Segment. The tool should be able to automatically find and track the valves, as well as automatically detect flow through the valves. It should also provide the user with blood flow measurements and a flow curve. The project was divided into the following objectives:

- Evaluate pre-implemented machine learning networks for valve tracking.
- Integrate valve tracking in the 4D flow module in Segment.
  - Write an algorithm for automatic segmentation of areas of valve flow in velocity images extracted from the MRI phase data.
  - Make the valve tracking tool as automatized as possible, but include opportunity for manual adjustment for user.
  - Consider user experience and make it intuitive and as fast as possible.
- Validate solution against a variety of data. The validation process should include data from patients of different sex, age and heart conditions, as well as images from different MRI machine vendors.
- Consider the common problem of misaligned 2D and 4D data and explore possible solutions for automatic or manual correction.

3

Background / Theory

3.1 Cardiac anatomy and physiology

The heart is the organ responsible for pumping blood throughout the body. The heart is divided into four chambers as can be seen in Figure 3.1. The atria, the two upper chambers, receive blood from the body. The ventricles, the two lower chambers, pump the blood out of the heart. The right half of the heart is responsible for handling deoxygenated blood, where the right atrium receives the blood from the body and the right ventricle pumps the blood to the lungs for oxygenation. The left half of the heart receives oxygenated blood from the lungs into the left atrium and then the left ventricle pumps the oxygen-rich blood out through the aorta to the rest of the body. [2]

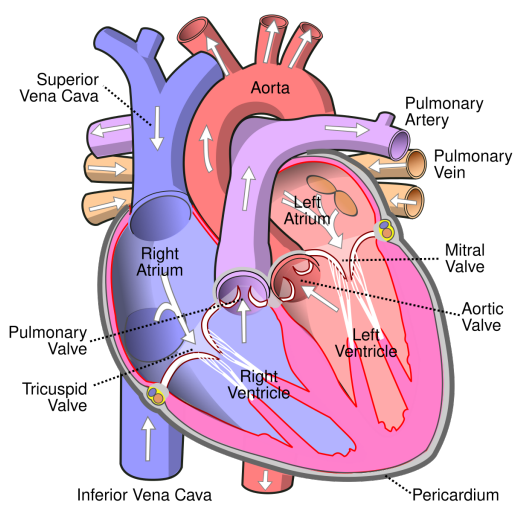

Figure 3.1: Diagram of the human heart. [3]

The atria and ventricles are separated by the atrioventricular valves to ensure one-way flow through the heart. The right chambers are separated by the tricuspid valve, while the left chambers are separated by the mitral valve, as seen in Figure 3.2. The mitral and tricuspid valves prevent blood from flowing back into the atria during systole when the heart contract. During diastole, when the heart relaxes, the mitral and tricuspid valves open and allow flow from the atria to the ventricles. The mitral valve is located postsuperior in relation to the tricuspid valve. The fibrous ring forming the orifice of the mitral valve has a circumference of around 7-9 cm, while the tricuspid has a greater circumference ranging between 10-11 cm. The annulus (ring) of cartilage changes shapes during the different stages of the cardiac cycle. For the tricuspid valve the changes are more pronounced where the ring changes shape from circular to elliptical. [2], [4], [5]

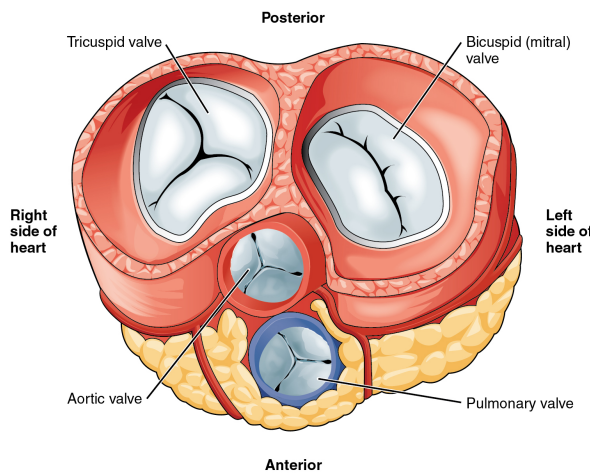

Figure 3.2: Heart valves diagram. [6]

During the early stages of the ventricular diastole the pressure in the ventricles decreases, while the pressure in the atria increases during the filling of the atria. When the atrial pressure becomes higher than the ventricular pressure, the AV valves open and the blood flows from the atria to the ventricles freely due to the pressure difference. This passive filling is referred to as the ventricular filling, and corresponds to approximately 70-80% of the filling of the ventricles. During the later stages of the ventricular diastole, the atria contracts and pump the remaining 20-30% of the blood into the ventricles. [7]

3.2 Valve disease and medical background

Valvular diseases, with compromised function of the valves, are commonly characterized by the inability of the valve to completely open or close. The valve dysfunction of failing to fully open during diastole is called stenosis. In atrioventricular (AV) valves

stenosis results in restriction of the blood flow from the atrium to the ventricle. The valve dysfunction of failing to fully close during systole is called insufficiency and results in regurgitation. For atrioventricular (AV) valves regurgitation means that the blood flows back into the atrium from the ventricle. Regurgitation causes a lower cardiac output and increase the pressure in the atrium [4]. According to guidelines from the American Society of Echocardiography [8], the severity of regurgitation can be classified as mild, moderate or severe. Regurgitation in the mitral valve is considered mild for a regurgitation volume (RVol) of <30 ml and regurgitation fraction (RF) of <30%. It is considered moderate for a RVol of 30-59 ml and RF of 30-49% and severe for RVol ≥60 ml and RF ≥50%. For the tricuspid valve, a RVol of <30 ml is considered mild regurgitation, while moderate for 30-44 ml and severe for ≥45 ml.

When valve dysfunction is suspected, valve diseases can be diagnosed by initially performing a physical examination, a heart sound and murmur examination and reviewing patient history. To confirm the diagnosis the most commonly used imaging modality is 2D Doppler echocardiography to assess the function and anatomy of the valves. A transthoracic echocardiogram gives information about the structure of the heart, chambers and valves as well as size of the chambers and heart walls. Combined with a Doppler, the flow through the heart and valves can be studied. In cases where a transthoracic echocardiogram is not sufficient for diagnosis, transesophageal echocardiography or cardiac magnetic resonance imaging (CMR) can be used instead. [4], [9], [10]

3.3 Magnetic Resonance Imaging

Magnetic Resonance Imaging (MRI) is a non-invasive imaging technique that can be used for medical imaging of organs in the body without using radiation. The fundamental basis of MRI physics is based on the nuclear magnetic resonance property that atoms with an odd number of protons, such as hydrogen with one proton, have in a magnetic field. These atoms have positive electrical charge and spin, creating a local magnetic field. When applying a strong external magnetic field (B_0) the protons align with the longitudinal direction of the magnetic field. The alignment of the protons results in a net magnetic vector in the direction of the B_0 magnetic field. To measure the net magnetic vector a radio-frequency (RF) pulse is applied to excite the protons and flip the net magnetic vector into the plane perpendicular to the external magnetic field (B_0). When the RF pulse is switched off, the protons relax and the net magnetic vector returns to the resting state in the direction of the B_0 magnetic field. It is the energy that is released when the protons relax, that is detected as the MR signal by RF coils in the MR scanner. The difference in relaxation times between different tissues, creates the contrast differences between different tissues and organs in MR images. [11], [12], [13]

3.3.1 Cardiovascular Magnetic Resonance

Cardiovascular Magnetic Resonance Imaging (CMR) is a specialized technique of MRI adapted for imaging of the heart and vascular system. The challenges that CMR has to take into account and adapt the principles of MRI for is the cardiac and respiratory motion. The respiratory motion is mainly minimized by breath holding during image acquisition. However, respiratory gating can also be used to correct artifacts from breathing motion or when breath holding is not possible. Cardiac motion is compensated by using cardiac gating were the acquisition of images is synchronized to the cardiac cycle in an ECG. [12], [14]

Examples of standard image views for cardiac 2D images are left ventricle two-chamber (2CH) and four-chamber (4CH) views of the heart. In the 2CH-view (see Figure 3.5a), the image is acquired with a plane passing through the left atrium, mitral valve, left ventricle and apex of the left ventricle to create a view of the two chambers in the left side of the heart. The four chambers of the heart are captured in the 4CH-view (see Figure 3.5d) by acquiring the image with a plane the passes through the four chambers, the mitral and tricuspid valves and the apex of the heart. [14], [15]

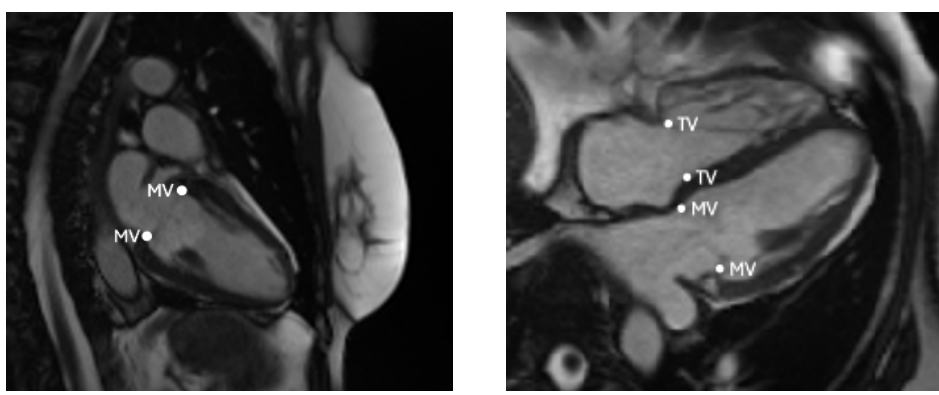

(a) 2CH view of heart, with mitral valve (MV) points marked

(b) 4CH view of heart, with mitral valve (MV) and tricuspid valve (TV) points marked

Figure 3.3: Standard views of cardiac MRI

To visualize and follow the motion of the heart throughout the whole cardiac cycle cine MRI is used. Cine MRI is a specialized MRI technique that captures a cinematic image set of the dynamic processes of organs in the body and displays the cine images in a playing loop. To capture cardiac cine images, data is acquired of the different phases of the cardiac cycle over multiple heart beats. The image frames in the cardiac cycle of a cine image is reconstructed with the data from different heart beats. Compared to a standard static MR image that shows the anatomical structures, a dynamic cine image shows motion of the tissue and fluid. This provides information about the function of the heart throughout the cardiac cycle. [14], [15]

3.3.2 Phase-Contrast MRI

Phase contrast MRI (PC-MRI) is used for flow quantification. PC-MRI generates phase contrast images encoded with the velocity by acquiring with a flow-sensitive gradient. The phase coded images are generated by first acquiring a regular amplitude image and then followed by another acquisition with flow sensitivity activated. The phase difference between the two acquisitions is then calculated which reflects the velocity. The flow-sensitive gradient is applied in the spatial direction of interest. Movement and flow in the direction of the gradient gives a phase shift that is proportionate to the velocity, while stationary tissue or fluid shows no phase shift. Stationary tissue and fluid will appear gray in a phase contrast image, while flow through the plane will appear white or black depending on the direction through the plane. [14], [16], [17]

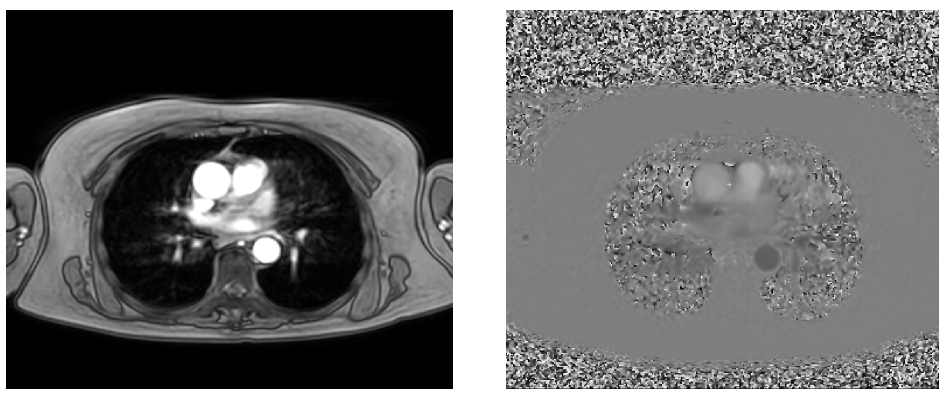

(a) Magnitude image (b) Phase image

Figure 3.4: 2D PC MRI magnitude and phase images.

3.4 4D Flow MRI

4D Flow MRI is a technique that generates time-resolved 3D image volumes by combining the techniques of Cine MRI and phase contrast MRI. The four dimensions of 4D flow include three spacial dimensions for the velocity measurements in the PC-MRI and a fourth dimension for time. 4D flow CMR is, according to the 4D flow cardiovascular magnetic resonance consensus statement from 2015 [18], defined as ”three-dimensional (3D) cine (time-resolved) phase-contrast CMR with three-directional velocity-encoding”. The three-dimensional velocity encoding in every point of the three-dimensional volume makes it possible to quantify blood flow in every direction. The temporal dimension makes it possible to follow and measure the flow throughout the cardiac cycle, which provides the availability to measure flow rate, forward flow and regurgitation.

The acquisition and workflow of 4D flow CMR images differs slightly from a 2D PC-CMR acquisition. Instead of acquiring the images during approximately 10-15

seconds and a single breath-hold like for 2D images, the 4D flow scan time is several minutes (5-8 minutes) with free-breathing. This can require additional gating to the respiratory cycle to compensate for movement or breathing. [16]

One of the advantages of 4D flow MRI is the ability to retrospectively access the velocity data in the entire volume of the 4D flow image. In 2D PC-MRI the plane of interest has to be chosen prospectively of imaging to apply the flow sensitive gradient correctly during the acquisition. The advantage of having the entire velocity data of the volume is that planes can be added retrospectively in regions of interest to calculate and quantify the flow in that specific area. [16]

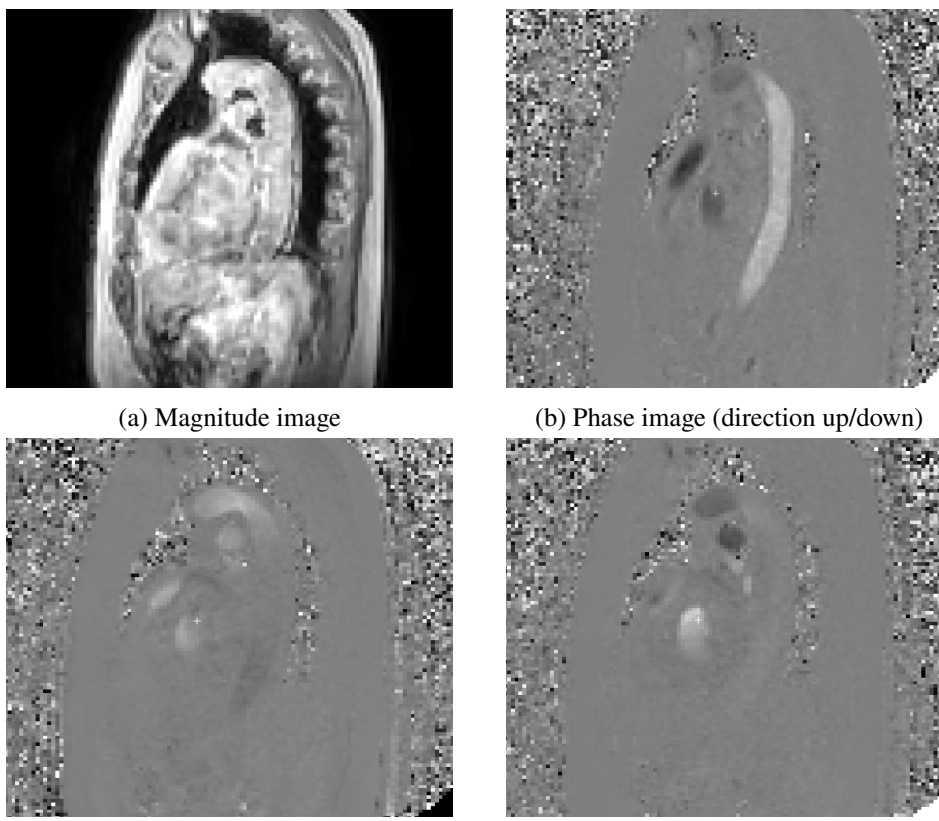

(a) Magnitude image

(b) Phase image (direction up/down)

(c) Phase image (direction left/right)

(d) Phase image (direction through plane)

Figure 3.5: 4D PC MRI magnitude and phase images.

3.4.1 Flow calculations

Flow is defined as the amount of fluid that passes through a surface or area during a given time. The flow through a plane or region of interest is calculated by taking the product between the velocity component that is perpendicular to the plane and the area of the plane. [19]

In the 4D flow CMR images, the velocity component perpendicular to an applied plane can be calculated from the three-dimensional velocity measurements of each voxel in the volume. In cardiovascular analysis of 4D flow CMR images, the flow through a vessel, chamber or valve can be calculated by applying a 2D plane across the region of interest. The flow through the region of interest (ROI) is calculated as the sum of the flow through all the voxels within the ROI, where each voxel's flow is calculated with the voxel's velocity component perpendicular to the applied plane and the area of each voxel. For flow estimation a deviation of $\pm 15^{\circ}$ of the imaging plane is tolerable. [18], [19], [20]

3.5 Valve tracking

Valve flow is investigated during assessment of valvular diseases and can be done using MRI. To quantify the flow, the position of the valve needs to be tracked throughout the cardiac cycle to know where to measure flow. Valve tracking can be performed retrospectively after imaging. For the valve tracking, two 2D images captured from different angles, optimally orthogonal views, should be used for each valve to capture the geometry. The 2D cine images will provide clear view of the anatomy for tracking the valves throughout the whole cardiac cycle, either manually or automatically. A neural network can be used for automatic tracking. The atrium and chamber will expand and contract at different stages, resulting in varying appearances of the heart which the network needs to be able to recognize. A 2D plane of thorough-plane velocities can then be reconstructed from the 4D data in the position of the valve for flow analysis. For a stationary plane, the velocities can be derived directly using the 4D flow data but a moving valve plane will move up and down through the blood volume to be measured. To isolate the blood's movement and capture the full blood volume, the velocity of the plane needs to be subtracted from the velocity data. [21]

Before valve tracking is performed the 4D flow data requires correction for phase offset errors caused by eddy currents which are loops of current induced by the rapidly switching gradient magnetic fields during MR imaging. These currents introduce image artifacts. This can be done as a post-processing steps after imaging where static-tissue interpolation offset correction is performed. It is recommended that both linear and polynomial fits to static tissue is readily available in the system. The phenomenon of velocity aliasing should also be considered as velocities surpassing the chosen velocity encoding (VENC) will result in corrupted flow results. Any misalignment between the 2D and 4D data should be corrected, either manually or automatically, for accurate valve tracking and flow measurements. In case of found evident regurgitation it is recommended to place a separate plane perpendicular to the regurgitant jet for a more precise regurgitant flow quantification. [21]

3.5.1 Previous research on valve tracking

In an article from 2001, Kozerke et al. discusses the use of the moving slice imaging method for the quantification of mitral and aortic regurgitation. The moving slice imaging method is performed during imaging where a reference point is selected, in this case the valve, and then the RF-pulse is varied to select different slices to follow the reference. This study showed that valve tracking is particularly important in mild to moderate regurgitation where adjusted measurements differed significantly from static measurements. [22]

Westenberg et al. published an article in 2008 about the accuracy of 3D velocity encoded MRI for blood flow quantification in the mitral and tricuspid valve. The study included flow data collected in both 2D and 3D from both phantoms and patients. The study found that both 2D and 3D imaging is accurate for flow measurements for a static plane with no in-plane motion. They also found that 3D flow imaging yielded accurate values in the presence of valve regurgitation and was more precise than the 2D method. [23]

In 2020, Blanken et al. compared flow quantification for semi-automated valve tracking and flow tracking in the presence of regurgitation. They found that a more accurate flow value could be produced by finding and tracking the backflow jet and measuring flow some distance away from the valve where the flow is more coherent. Flow tracking performed better overall compared to valve tracking, particularly in cases of severe valve regurgitation. [24]

In the ”4D Flow cardiovascular magnetic resonance consensus statement” from 2023 Bissell et al. outlines guidelines for how to work with 4D flow imaging. In the section about valve tracking they describe how a 2D plane for flow measurement can be created by tracking valve points in two 2D cine images captured from different angles. These valve points are then transferred to the 4D space to create the 2D plane from the 4D velocity data from which the flow can be derived. A known error is misalignment between the 2D cine and 4D cine images and they also note that this needs to be resolved by by manual or automatic image registration. [21]

3.6 Machine learning

Machine learning is a field of artificial intelligence focused on developing algorithms to recognize patterns in data for prediction and decision-making. It is an important tool that can be used to automate time consuming tasks and analyse large amounts of data to detect patterns and trends. The objective is to create an algorithm that can be used on new unseen data, and to be able to do that it needs to be trained on relevant data from which it can learn. The training process can both be supervised or unsupervised. Supervised learning means that the algorithm is trained on data where the desired

output is known for each input. This approach works well for image analysis tasks such as object classification where there is a known desired output that the system should be trained to identify. This requires data that has been labelled with what is considered the ground truth. Unsupervised learning does not use pre-labelled data and can instead be used to identify hidden patterns in the data. [25]

3.6.1 Neural Networks

Neural networks is a machine learning method. The name comes from the structure of the algorithm which is resemblant of the neural pathways in the body. A neural network is comprised of a number of so called neurons. In its simplest form it has an input layer which receives data and distributes it, a hidden layer with nodes which perform computations on input data and an output layer. A network with multiple hidden layers is considered a deep learning network. For more complex tasks like object identification in images several hidden layers are needed. It is within these hidden layers that the network learns. The first layers after the input capture basic patterns in the data while recognition of more complex features are introduced in deeper layers. [25]

3.6.2 Convolutional neural networks

Convolution neural networks are a type of deep learning neural networks that are specialized in image processing tasks and visual pattern recognition. There are three types of hidden layers in between the input and output. The convolutional layer applies filters to extract features such as edges and texture, pooling layers downsamples to reduce dimensionality and fully connected layers take the downsampled feature maps of the other two layers and produce the final output. By combining these layers the network can learn complex representations of the input data where simple patterns are combined into more complex structures across the network. [25]

3.6.3 TVnet & MVnet

TVnet is a model trained to detect points for the tricuspid valve in 4CH cine MR images. A pre-trained version of ResNet-50, which is a deep convolutional network, was used as a base. To train and test the model 4170 images from a cohort of 140 patients with diverse cardiovascular conditions were used. The patients were scanned on a 1.5T or 3T Siemens MRI scanner. Two points were manually placed in each temporal frame by one researcher on either side of the tricuspid valve where it intersects with the right ventricular myocardium. This was used as ground truth in the training process. The detection uses two networks where the first takes the original images and finds an approximate location of the points. This approximate location is then used to ensure the input for the second network is standardized in terms of size, cropping, resolution, and heart orientation. The second network then finds a more precise location of the two points. [26]

MVnet is trained to detect points for the mitral valve in both 2CH and 4CH cine MR images. It is based on TVnet and the pipeline is the same with two stages of networks for detection of the two valve points. This model used 38854 cine images from 703 patients to train and evaluate the model. The data spans various cardiac pathologies and includes scans from Siemens, Philips, and General Electric systems. The manual annotation of ground truth images were done by 10 observers where points were placed in all time frames for 458 subjects and only at end-diastolic and end-systolic frames of 245 subjects. [27]

3.7 Validation

Any newly implemented flow quantification method for clinical 4D flow CMR needs to be validated to ensure it meets quality thresholds. 4D flow CMR can be compared to 2D flow CMR where forward volume for one cardiac cycle should be compared between the two for the aorta and the pulmonary artery. A within data set validation of 4D flow should also be performed. Aortic volume can be compared to pulmonary volume where it should differ 5%. Flow quantification of backflow with valve tracking can be validated against standard methods. If significant differences in resulting regurgitation volumes is found, the new method should be revised. Discrepancies of >15 ml or >10% should be cause for concern. Ideally differences between methods should be less than 5% [21]. To validate the method a variety of data should be used. The method should be tested on hearts with different cardiovascular conditions as well as healthy hearts for female and male, adults and children. It should also be evaluated on images from different scanner vendors.

A way to use 4D flow data to validate the results of the valve tracking flow analysis for the mitral valve is to find the aorta inflow by placing a plane at the base of the aorta, and then compare it to the flow through the valve tracking plane. These values should approximately be the same. For the tricuspid valve the flow can be compared to the inflow to the pulmonary artery. An alternative way to obtain flow through the aorta and pulmonary artery is to measure it in 2D short axis cine images or in 2D transversal images showing the aorta and pulmonary artery.

3.8 Segment

Segment is a software for visualization and analysis of medical images developed by Medviso AB for both research and clinical purposes. Segment provides tools for quantitative analysis of medical images, particularly in cardiac magnetic resonance (CMR), supporting measurements such as ventricular volumes, ejection fraction, strain, and flow. Segment CMR is the clinically approved version of the software used in routine clinical workflows, and it includes selected functionalities of the research available

version of Segment. Some of the key features of Segment are AI-based automatic segmentations of the heart chambers from CMR images, automatic vessel tracking and flow analysis tools. One of the modules included in Segment is a module for 4D flow analysis. In the 4D flow module flow visualizations and measurements can be made from 4D flow MRI data. [28]

4

Methods

The structure of the flow quantification tool is illustrated in Figure 4.1. The methods section is divided into sections that describe each component of the tool, its integration into the Segment software, and the final validation procedure.

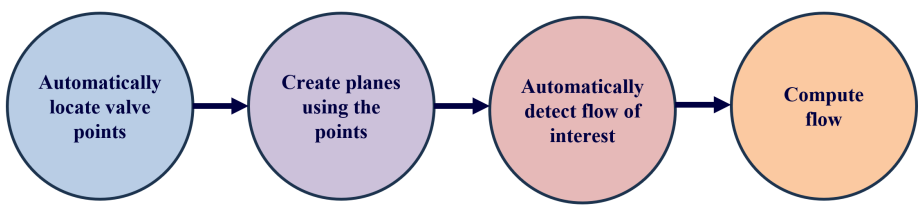

Figure 4.1: Flowchart describing the structure of the flow quantification tool.

4.1 Valve tracking

Points for the mitral and tricuspid valves for the entire cardiac cycle were determined using pre-trained machine learning networks. Two different tracking algorithms were tested. The first algorithm had been trained to segment the four chambers of the heart and the myocardium of the end-diastole time frame. From these segmentations points for the mitral and tricuspid valves could be extracted. A script was created to perform the tracking in all time frames and was tested on multiple data sets. The tracking failed for at least one time frame in an unacceptable amount of data sets, deeming the algorithm unusable for valve tracking. The second algorithm uses the pre-trained convolutional neural networks MVnet and TVnet to predict valve points in all time frames of the 2CH and 4CH cine images. This algorithm proved to be more successful in correctly placing the valve points. From the 2CH image the algorithm extracts and saves two points for the mitral valve in every time frame, while the algorithm for the

4CH image extracts and saves two points for the mitral valve and two points for the tricuspid valve.

If the automatic valve tracking fails in some time frames it is possible to move the tracked points in each individual time frame. There is also a function for AV-plane displacement analysis was already implemented in Segment that can be used for semi-automatic valve tracking. The user can then select one 2CH, 3CH and 4CH cine image and manually place markers in all three images for the mitral and tricuspid valves in one time frame. An algorithm then calculates the positions of the valves in all time frames [29]. If the fully automatic valve tracking using MVnet and TVnet fails, this semi-automatic way to find valve points can be used. Labels used internally in Segment for valve points found with MVnet and TVnet was intentionally set to be different than points found from the AV-plane displacement analysis. When the button for valve tracking in Segment's 4D flow module is pushed a check is performed to see if any valve tracking has been performed, and what type of valve tracking it was to provide the user with options of how to proceed.

4.2 Creating a plane

To create the valve tracking plane the following attributes of the plane needed to be calculated.

1. Two vectors defining the plane in every time frame
2. The normal of the plane in every time frame
3. Plane dimension
4. Four vertices (corner points) of the plane in every time frame
5. Plane position (starting point) of the plane in every time frame

With the valve points for the mitral and tricuspid valve from the valve tracking machine learning algorithm, the attributes of each respective plane were calculated. More detailed computations of each plane is presented in the respective Sections, 4.2.1 and 4.2.2.

All calculations and resulting values and attributes of the valve tracking plane were made in the RLAPFH-coordinate system. The RLAPFH-coordinate system is the coordinate system used in DICOM-images (Digital Imaging and Communications in Medicine) used to define the position and orientation of a image in relation to a scanned subject. RLAPFH gives the coordinates in a right-left (RL), anterior-posterior (AP) and feet-head (FH) coordinate system. Each image's internal xyz-coordinate system has a relation and reference of its points in the RLAPFH-coordinate system.

To ensure consistency and to get correct velocity direction throughout the time frames and data sets, the normals of the plane must be oriented in a same direction throughout all time frames. The reference direction of the normals was set in the head-to-feet direction to get positive flow direction through the valves. If the direction of the normal of the current time frame calculated was different to the reference direction, the normal was flipped to be the same direction as the reference.

Due the number of time frames often differing between the 2D and 4D data set, the normals, vertices and plane positions were resampled through interpolation to correspond to the 4D dataset.

4.2.1 Mitral valve tracking plane

For the mitral valve plane, the least square plane fitting method was used with the four mitral valve points to calculate the normal and center point of a plane fitting all the valve points, see Equation 4.1. With least square plane fit the normal of the plane was calculated using Single Value Decomposition (SVD) and the cross product of the left singular vectors. With the given points the mean coordinates (center point) was calculated and then each of the points were centred around the origin. The centred points coordinates were stored in a matrix A and were used in MATLAB's function SVD to calculate the left singular vectors of the matrix, U. The cross product between the left singular vectors gives the normal vector N of the plane.

$$\begin{gathered} x = [x_1, x_2, x_3, x_4] \quad y = [y_1, y_2, y_3, y_4] \quad z = [z_1, z_2, z_3, z_4] \\ A = [x; y; z] \\ A = U\Sigma V \\ N = U_1 \times U_2 \end{gathered} \tag{4.1}$$

The four mitral valve points were then projected onto the least square fit plane by first calculating the distance between the center point and each of the points. The distance to move the points in the direction of the normal during the projection was calculated by taking the dot product between the calculated distance to the center point and the normal of the plane, see Equation 4.2.

$$\begin{aligned} d_{\text{center}_i} &= \text{center} - P_i \\ d_{\text{proj}} &= d_{\text{center}_i} \cdot N \\ P_{\text{proj}_i} &= P_i - d_{\text{proj}} \cdot N \end{aligned} \tag{4.2}$$

From the projected mitral valve points, the most stable point, located at the septum in the 4CH image, was selected and two vectors were calculated to the two points in the 2CH image.

$$\begin{aligned} v_1 &= MV_{2CH_1} - MV_{4CH} \\ v_2 &= MV_{2CH_2} - MV_{4CH} \end{aligned} \tag{4.3}$$

The lengths of the vectors, v_1 and v_2, were calculated and the largest value was multiplied by a scale factor to ensure that the plane covers the entire valve opening. The scaled length of the plane was compared to the saved maximum length of the plane. If the scaled length was larger than the current maximum length the maximum length was replaced. After iterating through all time frames the maximum length of all the time frames was saved as the plane dimension of the mitral valve tracking plane, this ensures that the plane has a constant size that covers the valve opening in all time frames.

Since the vectors v_1 and v_2 were not orthogonal to each other, a vector perpendicular to v_1 was calculated by computing the cross product between the normal and v_1. The perpendicular vector to v_1 replaced v_2 as the new vector v_2 within the plane. The vectors v_1 and new v_2 were used to make the plane square when calculating the vertices of the plane. The normalized vectors of N, v_1 and v_2 were saved as the vectors for the plane in the current time frame.

After calculating the normal, the vectors within the plane (v_1 and v_2), the center point of each time frame and the plane dimension, the four vertices were calculated. The vertices were calculated from the center point applying a displacement in the positive or negative direction along the vectors v_1 and v_2, with the distance of half of the plane dimension in respective direction, see Equation 4.4.

$$V_i = \text{centerpoint} \pm \frac{\text{plane\_dimension}}{2} \cdot v_1 \pm \frac{\text{plane\_dimension}}{2} \cdot v_2 \tag{4.4}$$

The vertex point V_1 was chosen as the plane position which is the point from which the plane is defined.

4.2.2 Tricuspid valve tracking plane

For the tricuspid valve, only two valve points were obtained from the valve tracking. To calculate the normal, two vectors that lie within the plane were needed. The first vector was calculated by constructing a vector between the two tricuspid valve points in the 4CH image, using the point at the septum of the heart as the staring point. To calculate the second vector, an initial assumption regarding the tilt of the valve was made. With the assumption that the tilt of the tricuspid valve is approximately the same direction as the mitral valve, the second vector was calculated between the two mitral valve points from the 2CH image. The normal of the plane was then calculated as the cross product between the two vectors.

$$\begin{aligned} v_1 &= TV_{4CH_2} - TV_{4CH_1} \\ v_2 &= MV_{2CH_2} - MV_{2CH_1} \\ N &= v_2 \times v_1 \end{aligned} \tag{4.5}$$

No exact angle in relation to the mitral valve could be found in any literature, but from anatomical models the tricuspid valve seemed to be tilted with the anterior side further

down. Different tilts were tested to see how they affected the final flow measurements. The vector v_2 was tilted by displacing the anterior end point of the vector downwards an approximated distance along the direction of the normal. The normal was recalculated for the tilted plane with the cross product between v_2 and v_1. Tilting the plane slightly provided results more in line with what was expected when comparing to other flows in the data set. However it is important to note that the change in angle did not drastically impact the flow measurements.

The length of the vector v_1, the distance between the tricuspid points, was calculated and multiplied by a scale factor to ensure that the plane covers the entire valve opening. The length was saved as the new maximum length of the tricuspid plane if it was larger than the previously saved maximum. To ensure a constant size of the plane and coverage of the valve opening in all every time frames, the maximum length of all time frames was saved as the plane dimension.

To create a plane that is square, the two vectors that define the plane need to be orthogonal to each other. Since the two vectors, v_1 and v_2, were not orthogonal to each other, a vector perpendicular to the vector v_2 was calculated by computing the cross product between the normal and vector v_2. For the tricuspid valve plane the vector v_2 was chosen as the vector to create the orthogonal plane from, due to that giving the plane a orientation more comparable to the mitral valve plane. The orthogonal vector to v_2 replaced v_1 as the new vector v_1. The normalized vectors of v_1, v_2 and the normal N of each time frame were saved as the vectors of the tricuspid valve tracking plane.

The center point of the tricuspid valve plane was calculated by first finding the mid point between the two tricuspid valve points. Due to the 4CH image not crossing through the center of the tricuspid valve, this mid point did not represent the actual center point of the valve. The tricuspid valve is located anteroinferior in relation to the mitral valve. The point was then adjusted along the crossing vector v_2, with a scaled factor of the distance between the tricuspid valve points, see Equation 4.6. When not translating the center point of the plane towards the center of the valve, some of the flow through the valve was missed due to the plane not covering the entire valve opening.

$$\text{center} = \text{center}_{\text{TV}} - v_2 \cdot l_{TV} \cdot \text{factor} \tag{4.6}$$

The four vertices of the plane were calculated with the vectors defining the plane and the center point of each of the time frames and the plane dimension. Starting from the center point, a displacement of the half the plane dimension was added in the positive or negative direction along the vectors, v_1 and v_2, respectively, see Equation 4.4. The first vertex point V_1 was chosen as the the plane position from which the plane was defined.

4.3 Calculation of velocity images

A function for calculating a velocity image was already implemented in Segment for a stationary plane. This was used as a starting point and rewritten to work for the moving valve tracking plane where a 2D velocity image for each time frame was extracted from the 4D phase data in the position of the valve plane. The plane's origin was used as a base together with the plane's basis vectors to create a grid containing points. Each point, with coordinates in the patient coordinate system (RLAPFH), represents pixels in the image. All points were converted to Segments internal coordinate system and separated into x, y, z components. 3D image stacks with phase data in x, y, and z directions respectively were obtained and velocity information in all three directions were found for the points in the plane with interpolation. The found velocities were then projected to the plane normal to calculate the through plane velocities and produce a velocity image.

4.4 Automatic segmentation of region of interest for flow analysis

The velocity images were used to find and define a region of interest (ROI) for flow calculations. Only the valve area where flow should be measured is to be included in the ROI. The reference direction of the plane normal set when creating the planes ensures that normal valvular flow (from atrium to chamber) is positive. The algorithm for the mitral valve was created first and tested on the tricuspid but with poor results. Due to variations in velocity images across different datasets, the algorithm was continuously tested and refined throughout the development process to ensure that it could robustly handle different types of velocity images. Since the velocity images for the mitral and tricuspid valves differed where the tricuspid often had larger lighter areas that were not flow, two different segmentation algorithms were written. Both segmentation algorithms follow the same general structure. Details for steps 1-4 that differ between the algorithms are found in 4.4.1 and 4.4.2.

1. Define areas to search for flow

A circular area of where flow is expected to be was defined. For some datasets vessels could be found on the fringes of the plane and narrowing the search field ensures that high velocity area from such vessels are not mistaken as valve flow by the algorithm.

2. Segment areas with negative flow

Areas with negative velocities were segmented below a threshold to find interesting areas with negative flow in all time frames.

3. Segment areas with positive flow

Areas with positive velocities were segmented above a threshold to find an interesting area with positive flow. This was used as a fixed mask for all time frames.

4. Create the final mask

A mask for the (positive) valve flow was created where negative velocities that were not considered backflow through the valve were removed.

5. Exclude images with no flow

All negative velocity areas were removed from the positive velocity mask before a median was calculated. A median was then calculated for the background with no positive and negative velocity masked areas. The absolute difference between the medians was calculated to decide if a time frame had any flow of note to measure. The threshold was found by testing multiple data sets. If the background and positive flow mask were similar, the mask was replaced by the mask for backflow if there was one, otherwise with a point.

6. Find the boundary

The boundary was found for the final mask. The mask was padded to allow edge detection for masks extending to the border of the image which was removed after a contour had been determined.

7. Create the final ROI

The number of contour points were downsampled. The final number of visible points were set to be 12, fewer did not always capture the shape of the flow. A smoothing filter was applied in the spatial direction ensuring smooth transition of the contour which makes it resistant to sudden changes in the area of interest caused by artifacts.

4.4.1 Mitral valve

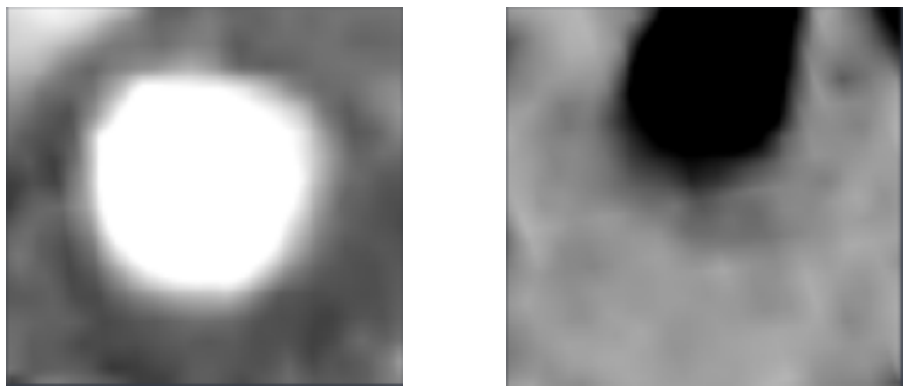

(a) Valve flow shown as positive (light) flow. (b) Aorta flow shown as negative (dark) flow.

Figure 4.2: Images showing velocity images from the same patient during different stages of the cardiac cycle.

1. Define areas to search for flow

The velocity images for the mitral valve shows both valve flow as well as aorta flow during different stages of the cardiac cycle. This can be seen in Figure 4.2 showing velocity images for the same patient for different time frames. As the heart beats the valve flow will expand, fade and then disappear as it is replaced by the start of aorta flow that will begin to expand. These flows will alternate during the cardiac cycle. Possible backflow (dark) through the valve will occur during systole when the aorta flow is visible. When comparing the flows in Figure 4.2 it is evident that the aorta flow will expand into the area where valve flow is seen, which is the area where regurgitation is expected to be. This makes it necessary to identify the aorta flow to separate it from possible backflow in the valve. For this reason two different circular areas for flow detection was created in step 1 of the algorithm. A smaller area was chosen to search for the maximum valve (positive) flow and a larger area was used to search for the maximum aorta (negative) flow as the aorta is closer to the image border. Both areas were saved as binary masks.

2. Segment areas with negative flow

The circle mask for the aorta was applied to all velocity images to exclude velocities outside of the search area. A Gaussian blurring filter was also applied. All these images were then searched to identify the maximum negative velocity, the Gaussian filter ensured a small speckle was not selected. This value was multiplied with a scale factor to create a global threshold. The scale factor was decided through testing. The negative velocities were then segmented in all time frames. The local maximum negative velocity was found and scaled for each velocity image and was compared to

the global threshold. If it was higher than the global threshold, indicating large gray areas with no interesting negative or positive flow, the global threshold was used on the image to avoid selecting gray areas. If it was lower, the local value was used instead for segmentation. Segmentations for all time frames were stored in a variable.

To identify the aorta, all velocity images were segmented using the global maximum velocity value with a scaling factor. The areas of regions in all the images were then calculated and the overall maximum area was identified as aorta flow and stored as a mask.

3. Segment areas with positive flow

The circle mask for the valve was applied to all velocity images. A Gaussian filter was applied before the maximum positive velocity in all images was found. This was scaled with a factor found through testing and used as a global threshold. Each image was then thresholded to identify positive flows. The local maximum positive velocity was found and scaled for each velocity image and was compared to the global threshold. If it was lower than the global threshold, indicating large gray areas with no interesting negative or positive flow, the global threshold was used on the image to avoid selecting gray areas. If it was higher, the local value was used instead for segmentation. The position of the global maximum velocity was used to select areas that belong to the valve flow. These areas were then stacked upon each other to cover the entire valve area and create a mask.

4. Create the final mask

For each image a final mask was created to determine the ROI, see Figure 4.3. The final mask was the mask for the positive velocities with negative velocity objects considered aorta or other flow excluded, and potential regurgitation included. Which parts of the negative velocity mask to include were decided by reviewing each separate object in the masks. For each object overlap was checked with the mask for the aorta, if overlap was found that area was excluded. If overlap between the object's centroid and the positive velocity mask was found it was included as that could be backflow. The centroid was used instead of simple overlap as there could be darker areas on the edge of the positive flow that should not be included. Other objects were excluded.

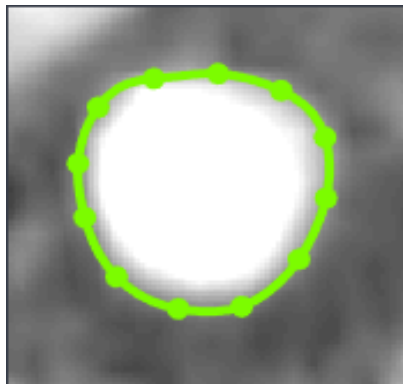

(a) Valve flow shown as light (positive) flow.

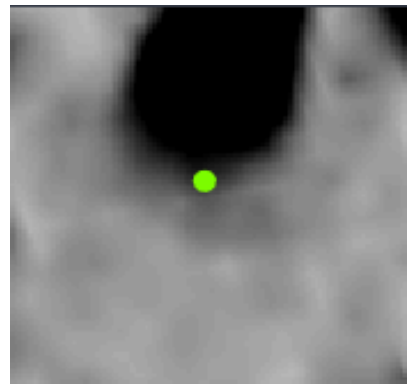

(b) Aorta flow shown as dark (negative) flow.

Figure 4.3: Images showing velocity images from the same patient during different stages of the cardiac cycle. The automatically detected ROI in seen in green. For (a) the ROI encompasses the valve flow, in (b) it is only a dot since no valve flow is found.

4.4.2 Tricuspid valve

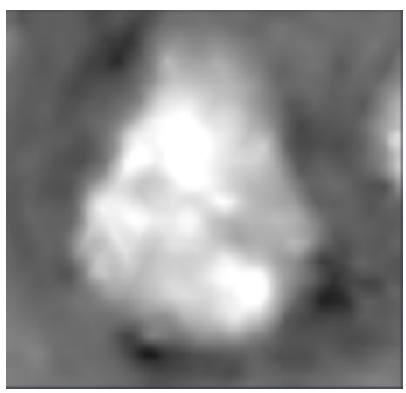

(a) Valve flow shown as positive (light) flow.

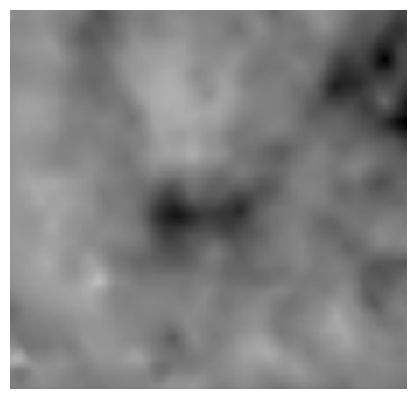

(b) Negative (dark) flow. In the center is backflow through the valve, to the upper right is flow from the pulmonary artery.

Figure 4.4: Images showing velocity images from the same patient during different stages of the cardiac cycle.

1. Define areas to search for flow

An example of velocity images from one data set is shown in 4.4. Positive flow through the valve can be seen in 4.4a. Figure 4.4b shows backflow in the center where the valve is, and flow to the pulmonary artery to the upper right which do not overlap with the valve area. Since no flows from larger vessels intrude the area of the valve,

no measures were needed to identify any specific regions of negative velocities to be removed. A circular area was defined for detection of positive valve flow.

2. Segment areas with negative flow

A Gaussian filter was applied to all velocity images and then they were searched for the overall maximum negative velocity. This value was scaled and used as a global threshold. For each frame the maximum negative value was found and scaled. Both scaling factors were found through testing. This value was compared to the global threshold and was used if it was lower, otherwise the global threshold was used to segment the image.

3. Segment areas with positive flow

A Gaussian filter was applied to all velocity images and then they were searched for the overall maximum positive velocity. This value scaled with a factor was used as a threshold. Only the frame with the maximum velocity was segmented and used as a mask. Several data sets had large light areas in some images that were not a part of the valve area that could be mistaken for such, which would have caused a to large mask if they were used. The frame with the maximum positive velocity should be when the valve is fully open and should therefore cover the appropriate area. The mask was dilated some to account for an eventual larger area in other images.

4. Create the final mask

A final mask was then created for each time frame to determine the ROI, see Figure 4.5. The negative velocity masks were searched for connected components and for each object it was decided if it should be included or excluded. A negative velocity object was considered backflow to be included if it's centroid was in the area of the positive velocity mask.

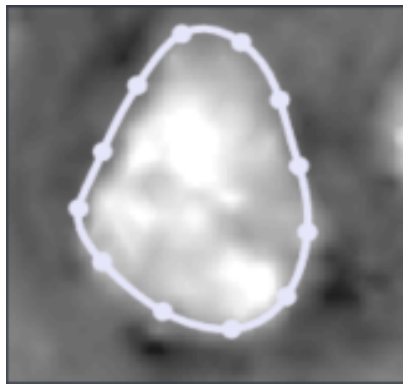

(a) Valve flow shown as positive (light) flow.

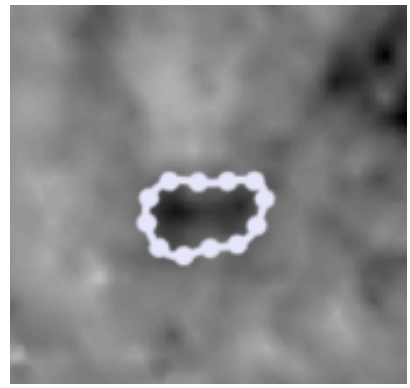

(b) Negative (dark) flow. In the center is backflow through the valve, to the upper right is flow from the pulmonary artery.

Figure 4.5: Images showing velocity images from the same patient during different stages of the cardiac cycle. The automatically detected ROI in seen in light purple. For (a) the ROI encompasses the valveflow, in (b) backflow has been detected.

4.5 Flow calculations

A function for calculating flow was already implemented in Segment for a stationary plane. This function was used as a starting point and was adapted for flow calculations of a moving plane. Before flow could be calculated for the moving valve tracking plane a compensation for the velocity of the moving plane needed to be made. This was needed to account for the volume of blood passing through the plane during the plane movement. The velocity of the plane in the current time frame was calculated by extracting the points within the planes at the time frames before and after the current frame. The distances between each of the points in the two time frames were calculated. The velocities of the points within the plane were calculated according to Equation 4.7 by taking the distances over the time, where dt is the time between two time frames.

$$v_{\text{tf}} = \frac{\text{points}_{\text{tf}+1} - \text{points}_{\text{tf}-1}}{2 \cdot dt} \tag{4.7}$$

For the first time frame the last frame was used as the previous plane. The first frame was used as the next plane for the last.

The plane's velocity components perpendicular to the plane were calculated with the dot product between the plane's velocity vectors and the normal of the plane. The perpendicular velocity component of the plane in each point, v_{plane}, was then subtracted from the through-plane velocity of each respective point in the velocity image, v_{image}. The new recalculated and adjusted velocity image of the plane in every time

frame was then used for the flow calculations.

$$v_{\text{adjusted}} = v_{\text{image}} - v_{\text{plane}} \tag{4.8}$$

The computed final velocity mask was applied to the adjusted velocity images to only calculate the flow for the velocity values inside the segmented region of interest. The flow, Q, was calculated in cm^3/s. The mean flow through the valve at each time frame was calculated, according to Equation 4.9, by the sum of all the masked velocities multiplied with the area of each pixel, A_{pixel}.

$$Q_{\text{tf}} = \sum(\text{mask}_{\text{tf}} \cdot v_{\text{adjusted}_{\text{tf}}}) \cdot \text{A}_{\text{pixel}} \tag{4.9}$$

For the positive flow only the positive velocities within the mask were used in the sum of the velocities. In similar a way only the negative velocities within the mask were used in the calculations of the negative flow.

The volume corresponding with the flow through the valve during the cardiac cycle was calculated in millilitres. The net volume was computed, as in Equation 4.10, with the sum of the mean flow in all the time frames multiplied with the time increment between time frames , dt.

$$V = \sum_{\text{tf}=1}^{N} Q_{\text{tf}} \cdot dt \tag{4.10}$$

The positive volume was computed by calculating the volume, according to Equation 4.10, with only the positive mean flows. The negative volume was calculated accordingly with only the negative mean flows.

4.6 Graphical functions and user interface

A view of the Segment 4D flow module is shown in Figure 4.6. In the middle a 3D vessel tree is shown. Three planes have been placed on the vessel tree. In the upper right corner an object list is found and below tools are found for the specific object that has been selected in blue in the list. Below a magnitude image (left) and a velocity image (right) of the selected plane is found. In the bottom right there is a flow curve and above it measurements are seen in a table. To the left there are different functions and tools that can be used in the module, and the valve tracking tool was added to this list. The implementation process included considerations related to both the graphical user interface and the underlying functions required to integrate the tool into the existing application. The following sections describe the different components and implementations related to the valve tracking tool, including what happens when the button is pressed and the functionality required to support the feature.

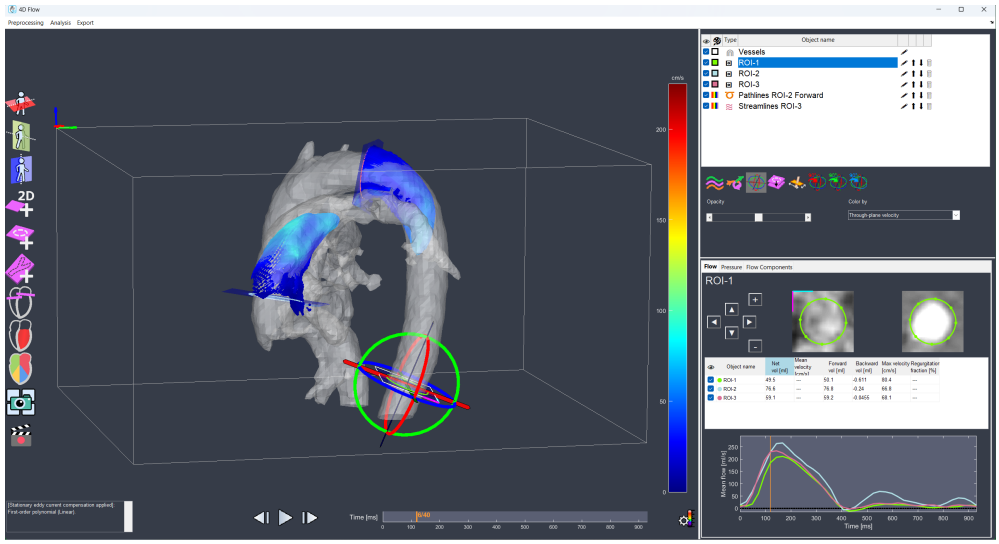

Figure 4.6: Segment's 4D flow module.

Adding the valve tracking planes to graphical interface

Once the mitral and tricuspid valve tracking plane objects have been created by clicking the valve tracking tool, they are added to graphical interface of the 4D flow module so they can be shown in the vessel tree. Each valve tracking plane is added the object list in the module where the user can select, modify and analyse the object. Measurements for each plane is shown in a table and flow curve.

Adding 2CH and 4CH images

In addition to the valve tracking planes, the 2CH and 4CH images are added to the graphical interface in the form of two planes. The planes are added to the object list, although initialized as not visible in the graphical 3D-space. The planes can be used when checking the movement of the valve tracking planes and visualize how the planes follow the valves in the anatomical cine images. The 2CH and 4CH planes are added automatically to avoid having the user add then manually and streamlining the analysis of the valve tracking.

Streamlines and pathlines

Streamlines and pathlines were functions already implemented in Segment for visualization of flow through a stationary plane. In Figure 4.6 the plane located furthest up has streamlines activated and the plane to the left has pathlines activated. With streamlines, flow can be visualized with arrows that show the direction and magnitude of the velocity in each pixel of the plane or region of interest for every time frame. With pathlines, the trajectory of particles seeded in the plane or region of interest at a

certain time frame can be followed showing how the particles move. The implemented functions for streamlines and pathlines were adapted to work for the moving valve tracking planes in addition to stationary planes.

Gimbal

Gimbal is another function already implemented in Segment for moving and rotating stationary planes. The gimbal feature can be seen in Figure 4.6 where it is activated for the plane furthest down in the image. For a stationary plane the plane position and plane vectors remain constant for all time frames. For the moving valve tracking plane the plane position and vectors are different for every time frame. The gimbal function of the valve tracking plane therefore had to be adapted to apply translation and rotation to each time frame accordingly to its plane positions and vectors.

ROI correction

Functions for correcting the ROI, such as translation and scaling of the entire ROI as well as moving single points on the ROI, are functions that were already implemented in Segment. However these functions needed to be adapted to work for the valve tracking plane. These functions allow the user to modify the automated segmentation in case it is needed. The ROI can be changed in the section shown to the middle right in Figure 4.6 where the magnitude and phase image is shown with the ROI. The ROI can be moved with the arrows och resized with the + and - buttons. The shape can also be altered by dragging the lines in the two images.

Change of colour bar scale

The already implemented colour bar for stationary planes had a range from zero to the positive velocity limit through the flow plane. The color bar can be seen to the right of the 3D vessel tree in Figure 4.6. For the valve tracking planes the range of the colour bar was changed to ± the velocity limit. This was done to visualize both positive forward flow as well as negative backward flow in the valve tracking planes.

Wait bars

The tracking process in the valve tracking algorithm, creation of the valve tracking plane objects and the graphical interface update were all process that were time-consuming. In total the process takes around 10-15 seconds. Loading the networks, MVnet and TVnet, takes an additional 15-20 seconds, but that is only done when valve tracking is run for the first time after launching Segment. Wait bars were therefore added for every process informing the user of progress for the process currently running. It was set up so that Segment will recognize when the networks have been loaded and can obtain them later to cut down run-time for subsequent runs. If the automatic valve tracking has been run on the data set the system will also recognize this and use the already detected points to further cut down on run-time.

Error messages and action prompts

The valve tracking algorithm requires at least one 2CH image and one 4CH image to run and predict the valve points. An error message was therefore added in case the user chose to run the valve tracking and the data set was missing any of the needed images, informing the user that the images are missing and to check the data set. In case that there are multiple 2CH or 4CH images, a message was added where the user is prompted to choose which of the multiple images they want to run the valve tracking on.

4.7 Alignment of 2D and 4D data

An attempt was made to create an algorithm for automatic alignment of 2D and 4D MR-images. A 3D image was created by extracting one time frame from the 4D data. The idea was to match the lungs in 2D and 3D magnitude images since they should have the same shape and size throughout the heart beat. A 3D magnitude image was collected from time frame one. 3D phase images were also created where flow could be found that could be matched with the 2D image. The 3D phase images were created by combining three 3D phase images with encodings in directions x, y and z. The velocities in each image were first centred around 0 and then squared to get the magnitude of the velocity. The final 3D phase image was then created by adding the three components and taking the square root of the sum. Time frames for peak ejection and peak filling were found in both the 2D and 4D stacks that could be compared and aligned for the phase images. Two different time frames were used to be able to compare suggested translation from the algorithm and check if they were similar. The heart will look a bit different in these two stages of the cardiac cycle and different flows will be visible in the phase images. During peak ejection, which is in between EDT and EST, there will be flow through the aorta. Between EST and EDT, during peak filling, there will be blood moving into the chamber that will show up light on the phase image.

A function was created that could extract an image slice for matching from a 3D space. A grid the size of the 2D image (x,y) was created and the z-value was controlled by an input to the function. A slice was then extracted from the 3D space where values were found by linear interpolation of each point in the grid and the 3D image. The slice was cropped to remove any undefined values. A function was then made for matching 2D and 3D magnitude images, and another for matching 2D images with phase images. An iterative search with offsets in the z-direction was set up where a slice was first extracted from the 3D space with an offset. This slice and the 2D-slice were then sent to separate image processing functions to create masks of interesting objects (lungs and flow). When masks had been retrieved for both images they were sent to an alignment algorithm. Several versions were made of this algorithm. The idea was to first create a distance landscape of the objects in the 2D image that could be used as a guide for translation and find the contour of the objects in the slice from

the 3D data. In one version of the algorithm the translation was found by iteratively moving the contours of the objects along gradients created from the distance landscape. For each iteration the contour was moved a fixed step length along the mean gradient in each direction (x,y). In another version a cost-function was created which calculated a cost based on the mean distance of all contour points for a proposed translation. An initial cost was calculated for the unmoved image. The translation was then found by iteratively calculating the cost of moving one step in the x-direction and the y-direction respectively. The cost at the beginning of the iteration was subtracted from these values to see if the translations was in the right or wrong directions. This information could be used for the next proposed translation to try to minimize the cost and find a final translation.
The automatic alignment function was ultimately not used since it was not robust enough.

A function for visualizing alignment of the 2D and 4D data was created in the Segment's 4D flow module. The user can press a button and a velocity image (from 4D phase data) will then be placed on top of the 2D cine images, allowing for quick assessment of alignment.

4.8 Plane to measure regurgitation

A function for creating a plane to measure regurgitation was created. A button can be pressed for either the mitral valve plane or the tricuspid valve plane to create a smaller static plane to measure backflow. Streamlines will also automatically be added for the valve plane so that the flow can be visualized. The plane for regurgitation measurements will be initialized with the gimbal function (for moving and rotating planes) to make it clear for the user that the plane should be moved to the area where backflow is.

4.9 Data

All data was pseudonymized prior to usage, removing any personally identifiable information. The data was checked for aliasing. Stationary eddy current compensation was applied on all data. In total 106 data sets from Siemens and 12 data sets from Philips were examined.

4.10 Validation

For validation, the following inclusion criteria for data were decided:

- Difference in blood volume for a cardiac cycle in the aorta and pulmonary artery in 4D vs 2D should be <10% or <15ml.
- No large areas of incorrigible aliasing caused by too low VENC.
- The aorta and pulmonary need to be distinguishable in the 3D vessel tree in Segment created from the 4D flow data.
- Aligned 2D and 4D data.
- A position without vortices needs to be identifiable to measure flow in the aorta and pulmonary artery.

Ideally the difference in volume between the aorta and the pulmonary artery in 4D flow data versus 2D flow data should be zero, but less than 5% according to the 2023 update of the 4D flow cardiovascular magnetic resonance consensus statement [21]. It also states that when comparing regurgitation methods the the difference between regurgitation volumes should be <10% or <15ml. While the difference between the aorta and the pulmonary artery in 4D versus 2D should be less, this threshold was set to allow for some errors in the measurement in 2D and 4D. The data used were not collected for this project, meaning that camera settings were not necessarily optimized for measuring the flow of interest for this project. A common issue found were a too low VENC resulting in aliasing, especially in the aorta where velocities are high. For some data the images were blurry due to patient movement during imaging. Data were excluded in cases where this resulted in the vessel tree not being cohesive enough to find the aorta and the pulmonary artery. Patient movement between the acquisitions of the 2D and 4D data can cause the 2D and 4D data to be misaligned. Cases with pronounced misalignment were excluded due to the tracked valve points of the 2D data not corresponding with the valve flow in the 4D data. In certain data sets assessment of aortic flow was difficult due to vortex formation, resulting in a loss of laminar flow in some places and therefore several planes needed to be checked. Some data sets were excluded due to it being to difficult to find a place with laminar flow. Table 4.1 shows the data used in the validation process.

Table 4.1: Table of data used for validation.

Vendor	Pathological group	n	Male	Female	Age
Siemens	Healthy adult	18	11	7	50±15
	Heart failure	12	4	8	67±8
	Healthy children	5	3	2	9±3
	ASD (postop) children	2	1	1	14.5±1
Philips	Mixed pathologies	7	3	4	50±18

Volumes corresponding to the net flow for one cardiac cycle were found for the mitral and tricuspid valve by running the valve tracking tool in Segment's 4D flow module. The automatically placed valve points found with MVnet and TVnet were checked against the 2D cine 2CH and 4CH images to see if they had been placed correctly and followed the valve's movement. The automatic flow segmentation were also checked in all time frames. Adjustments of the ROI were made if needed. Planes were placed in the aorta and pulmonary artery between their respective valves and where they branch off to measure the volumes for one heart beat. Several planes were placed for each to check for consistency in the same artery. The net volume in the mitral and tricuspid valve was used since that excludes any backflow and therefore is the amount that reaches the aorta. For the aorta and pulmonary artery the forward volume was used since that does not account for any possible backflow. The volumes for one heart beat in the aorta and pulmonary artery were also measured in 2D flow data data by using a tool in Segment to place a ROI on the vessel in all time frames. The forward volume was used from the 2D data.

The internal consistency of the data sets included in the validation cohort is shown in Table 4.2 and in the Figures 4.7-4.12. The consistency between the 4D and 2D of each included data set is shown in Figures 4.7-4.10, where the 4D aortic volume is compared to the 2D aortic volume and the 4D pulmonary volume is compared to the 2D pulmonary volume. The consistency within the 4D and 2D data sets are shown in Figures 4.11 and 4.12, where the 4D aortic volume is compared to the 4D pulmonary volume and the 2D aortic volume is compared to the 2D pulmonary volume.

Table 4.2: Table of mean and standard deviation of percentage difference between pairwise measurement comparisons of the data sets included in the validation across different vendors and in total. Number of data sets (n) are reported as Siemens/Philips/Total.

	Siemens	**Philips**	**Total**
Aorta 4D / Aorta 2D (%) [n = 36 / 7 / 43]	-1.03±6.43	-6.62±6.18	-1.94±6.65
Pulmonary 4D / Pulmonary 2D (%) [n = 22 / 7 / 29]	2.52±8.06	-6.79±8.77	0.35±9.02
Aorta 4D / Pulmonary 4D (%) [n = 35 / 7 / 42]	-7.17±10.84	-3.73±14.62	-6.59±11.42
Aorta 2D / Pulmonary 2D (%) [n = 24 / 7 / 31]	-5.62±5.42	-4.48±11.51	-5.36±7.02

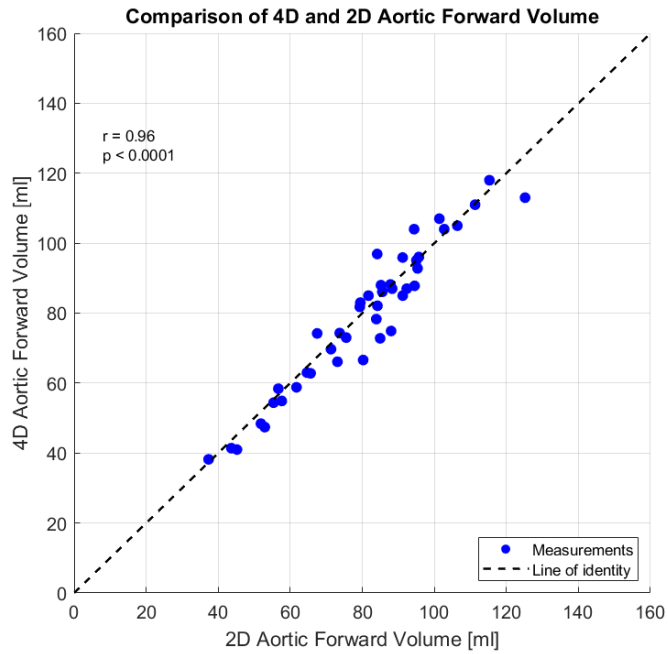

Figure 4.7: Scatter plot comparing the 4D and 2D aortic forward volume measurements of the data sets included in the validation.

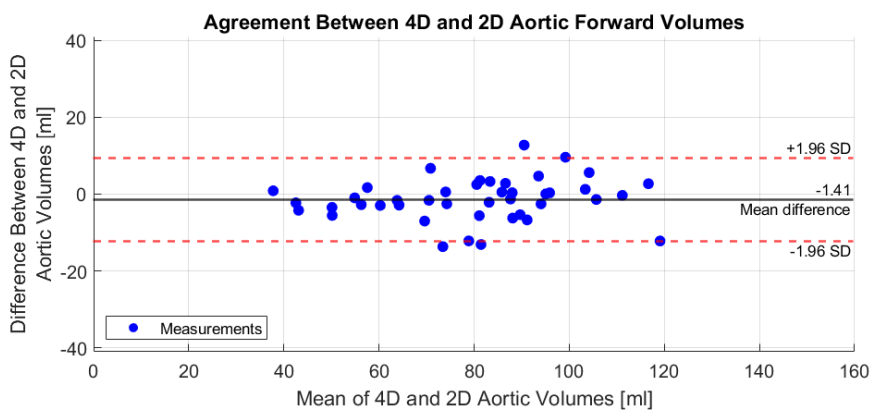

Figure 4.8: Bland-Altman plot showing the agreement between the 4D and 2D aortic forward volume measurements of the data sets included in the validation.

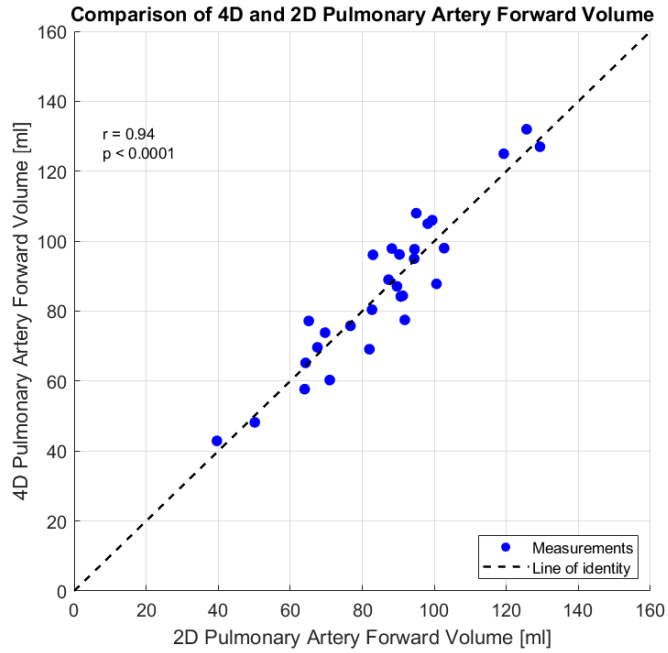

Figure 4.9: Scatter plot comparing the 4D and 2D pulmonary artery forward volume measurements of the data sets included in the validation.

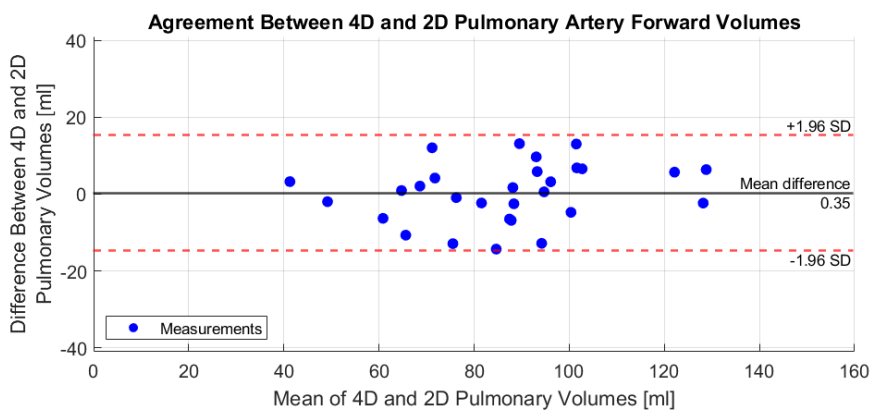

Figure 4.10: Bland-Altman plot showing the agreement between the 4D and 2D pulmonary artery forward volume measurements of the data sets included in the validation.

The scatter and Bland-Altman plots in Figures 4.7-4.10 and Table 4.2 of the differences between the 4D and 2D measurement confirm the fulfilment of the inclusion criteria for included validation data sets. Note that in Table 4.2, the standard deviation for the differences between 4D and 2D, when combined with the mean difference, extends

beyond the 10% limit of the inclusion criteria. However these data set were included as they still fulfilled the criteria of <15ml difference between the 4D and 2D measurement.

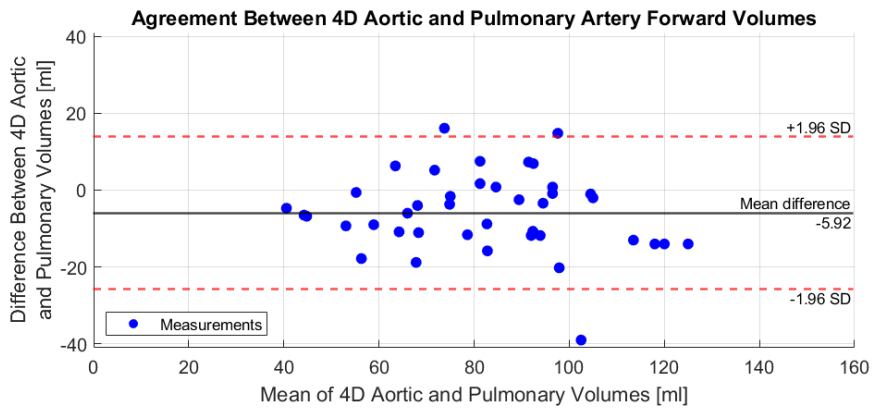

Figure 4.11: Bland-Altman plot showing the agreement between the 4D aortic and pulmonary artery forward volume measurements of the data sets included in the validation.

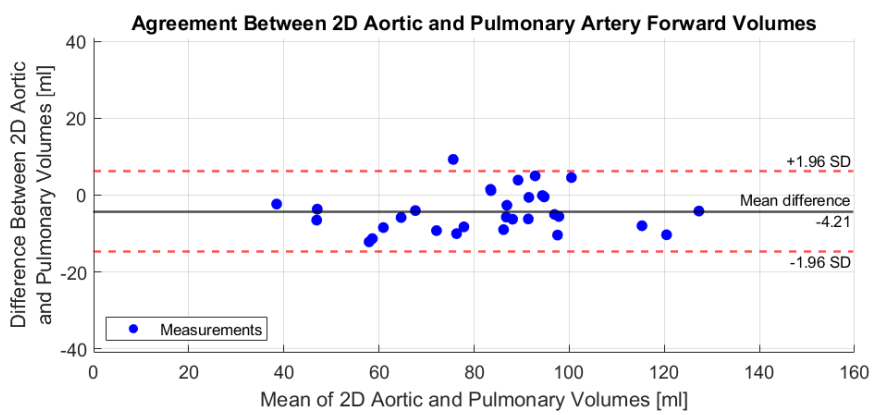

Figure 4.12: Bland-Altman plot showing the agreement between the 2D aortic and pulmonary artery forward volume measurements of the data sets included in the validation.

The Bland–Altman plots (Figures 4.11 and 4.12) and Table 5.4 for the validation included datasets show biases and percentage differences between aortic and pulmonary volume measurements consistent with an expected difference of approximately 5%.

Caas MR 4D Flow is a software from Pie Medical Imaging which has a valve tracking tool. A 2CH and a 4CH cine image can be used to track the mitral valve, and a 4CH image can be used to track the tricuspid valve. In Caas the tracking is semi-automatic where the user has to place points in the images in one time frame and the program

will then track the valves in the rest of the time frames automatically. A ROI will be initiated but will be the same for all time frames so it will need to be adjusted for each frame. Net volume was measured in Caas MR 4D flow for the mitral and tricuspid valves and the percentage difference between them and the values from Segment was calculated. A total of 8 data sets were checked where 6 were Siemens data (2 heart failure, 4 healthy) and 2 were Philips data (1 reduced ejection fraction, 1 increased septal wall thickness). After the workflow for valve tracking in Caas had been tested on a few different data sets the time to complete the valve tracking was recorded for 4 data sets. The time to run the valve tracking tool in Segment, including checking if the automatic segmentation was acceptable, was also recorded for the same data sets as a comparison.

5

Results

5.1 Mitral and tricuspid planes

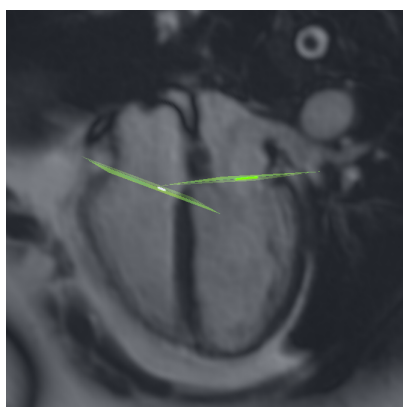

(a) Valve position end of diastole

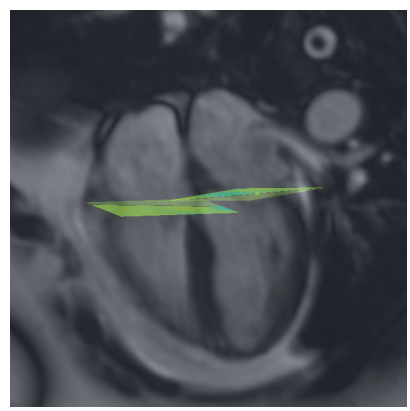

(b) Valve position during systole

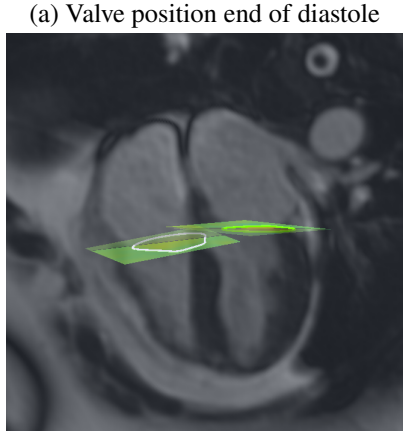

(c) Valve position during end of systole

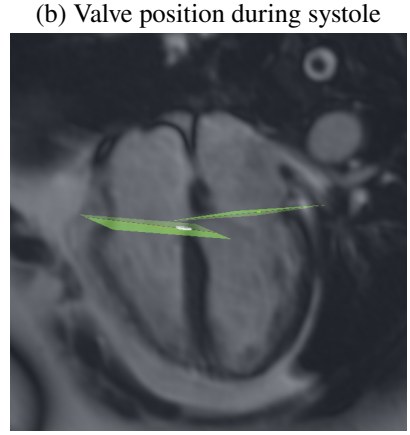

(d) Valve position during diastole

Figure 5.1: Images showing valve position with mitral and tricuspid valve tracking planes following the valve during different time frames of the cardiac cycle.

In Figure 5.1a, at the end of diastole, the valve tracking planes are located with the valves high towards the base of the heart, as the ventricles are filled with blood. During systole, in Figure 5.1b, the planes move down towards the apex, as blood is filling the atria as well as being pumped out of the ventricles. At the end of systole, the positions of the planes can be seen in Figure 5.1c. In Figure 5.1d, the valve tracking planes then move up towards the base of the heart during diastole, as the blood flows from the atria to the ventricles. From the sequence of images in Figure 5.1, it can be seen that the lateral parts of the valve tracking planes move more than the part of the planes located closer to the septum of the heart. This sequence of motion is repeated for every heartbeat throughout the cardiac cycle, with the valve planes continuously moving between the base and the apex as the heart contracts and relaxes.

5.2 Segmentation of velocity images

Two different segmentation algorithms were written for the mitral and tricuspid valves. Examples of automatic flow segmentations for the mitral valve are shown in Subsection 5.2.1. Subsection 5.2.2 shows examples of automatic flow segmentation for the tricuspid valve. The images shows how the automatic segmentation algorithms performed on data sets with and without regurgitation as well for images of varying quality. The flow curve for each data sets is also included where the mean flow is seen. The curve is expected to have two peaks during diastole corresponding to the periods of first and second filling of the ventricles.

5.2.1 Mitral valve

Velocity images for four time frames showing flow through the mitral valve are shown in Figure 5.2. Figures 5.2e-h shows the automatic segmentation of the blood flow, which can be compared to the unsegmented images in 5.2a-d. The flow curve for the data set with the different time frames marked out in coloured lines is seen in 5.2i. Time frames 3 and 11 have aortic flow shown as a dark area at the top and here no flow is measured which is confirmed in the flow curve. In time frames 27 and 37 there is blood flowing through the valve into the chamber, seen as a white area, which has been captured by the ROI lines. The flow curve shows that time frame 27 has a higher mean flow compared to frame 37, which also can be seen in 5.2g-h where frame 27 is brighter.

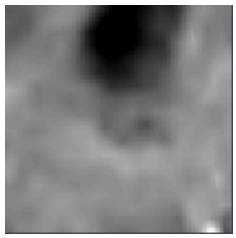

(a) Time frame 3

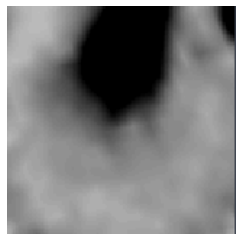

(b) Time frame 11

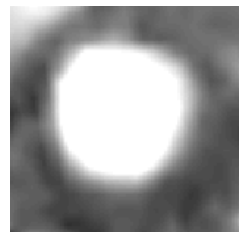

(c) Time frame 27

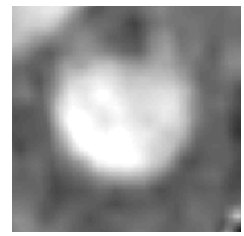

(d) Time frame 37

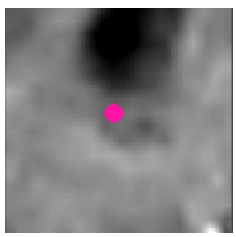

(e) Time frame 3

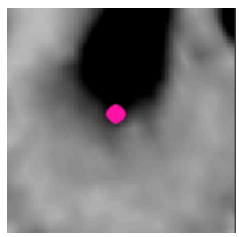

(f) Time frame 11

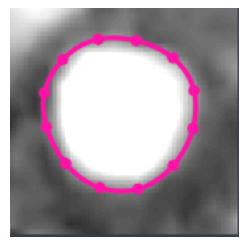

(g) Time frame 27

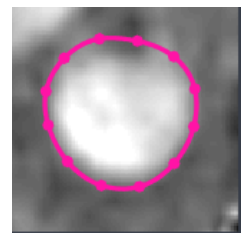

(h) Time frame 37

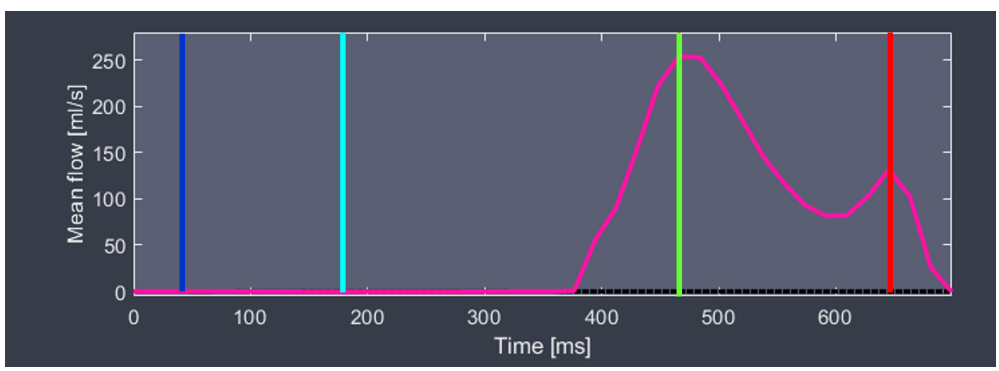

(i) Flow curve showing how the mean flow changes throughout the whole cardiac cycle. The coloured lines show time frames 3 (blue), 11 (cyan), 27 (green) and 37 (red).

Figure 5.2: Velocity images showing the mitral valve in four different time frames from a data set. The flow curve for the whole data set with the four time frames marked with coloured lines is seen in (i).

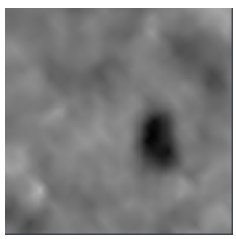

(a) Time frame 3

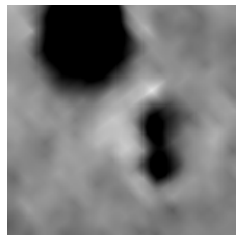

(b) Time frame 9

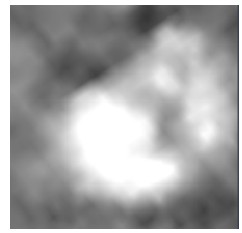

(c) Time frame 25

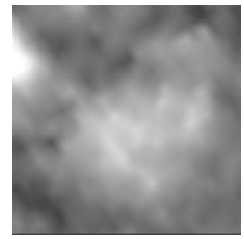

(d) Time frame 34

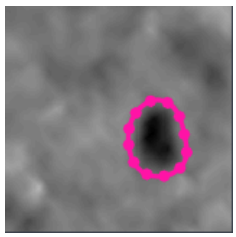

(e) Time frame 3

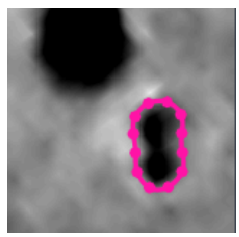

(f) Time frame 9

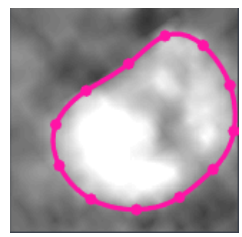

(g) Time frame 25

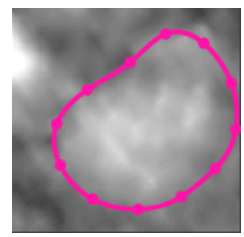

(h) Time frame 34

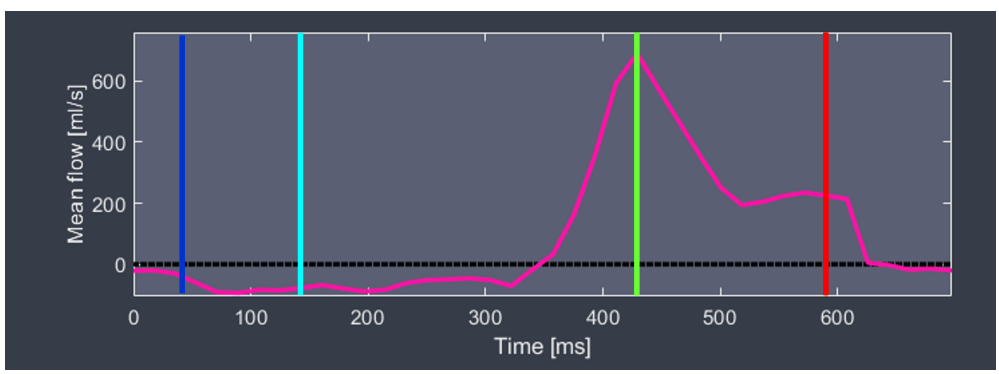

(i) Flow curve showing how the mean flow changes throughout the whole cardiac cycle. The coloured lines show time frames 3 (blue), 9 (cyan), 25 (green) and 34 (red).

Figure 5.3: Velocity images showing the mitral valve in four different time frames from a data set. The flow curve for the whole data set with the four time frames marked with coloured lines is seen in (i).

Four velocity images for four different time frames showing flow through the mitral valve are shown in Figure 5.3. Figures 5.3e-h shows the automatic segmentation of the blood flow and the unsegmented images can be seen in 5.3a-d. The flow curve for the data set is seen in 5.3i. Time frames 3 and 9 shows detected backflow. In time frame 9 aortic flow is seen at the top. The flow curve shows that backflow is detected the whole time during systole with the curve dropping below zero. In time frame 25 and 34 there is valve flow that has been detected. When comparing the two time frames in the flow curve it is clear that time frame 25 has stronger flow than 34, which is confirmed by the brightness of the flow in the velocity images.

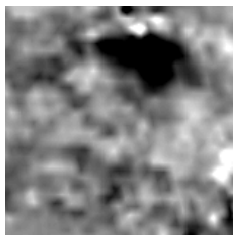

(a) Time frame 2

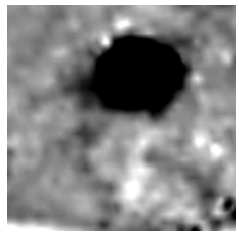

(b) Time frame 10

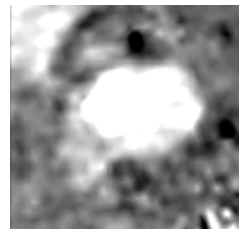

(c) Time frame 23

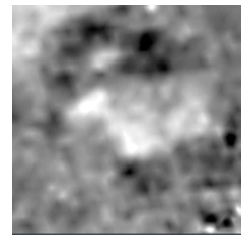

(d) Time frame 34

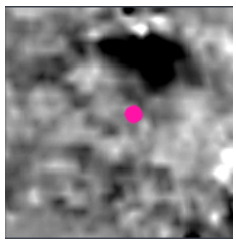

(e) Time frame 2

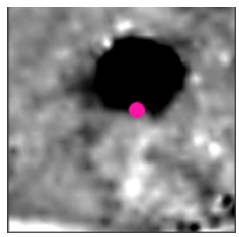

(f) Time frame 10

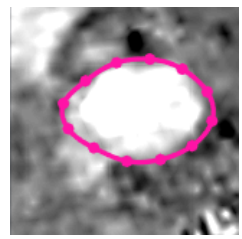

(g) Time frame 23

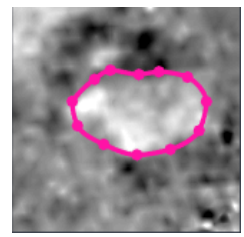

(h) Time frame 34

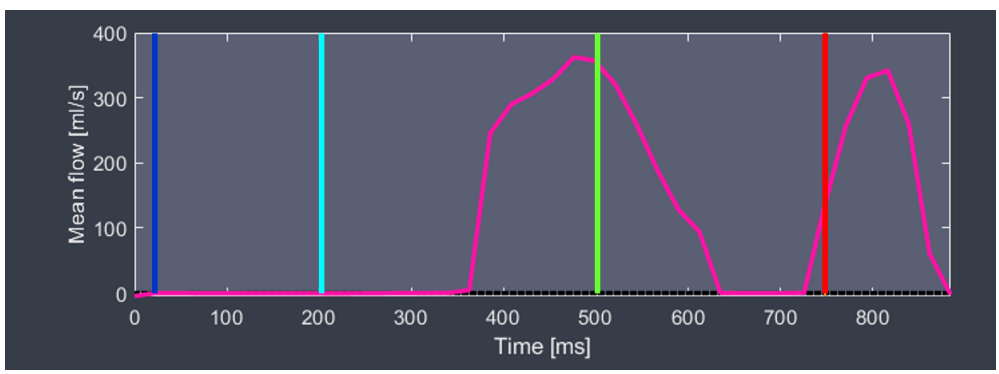

(i) Flow curve showing how the mean flow changes throughout the whole cardiac cycle. The coloured lines show time frames 2 (blue), 10 (cyan), 23 (green) and 34 (red).

Figure 5.4: Velocity images showing the mitral valve in four different time frames from a data set. The flow curve for the whole data set with the four time frames marked with coloured lines is seen in (i).

In Figure 5.4 velocity images showing mitral flow are shown. Unsegmented velocity images are shown in 5.4a-d and images with automatically segmented flow in 5.4e-h. There is only aorta flow in time frames 2 and 10 and the segmentation algorithm has reduced the ROI to a dot in these frames since there is no flow of interest. The flow curve in 5.4i shows that no flow is measured in time frames 2 and 10, while in time frame 23 and 34 there is valve flow. The data set is noisy with speckles. It is difficult to see the flow in time frame 34, but it seems like the ROI has missed some edges.

5.2.2 Tricuspid valve

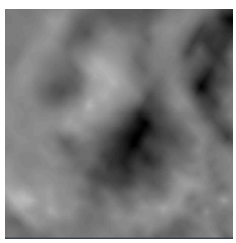

(a) Time frame 1

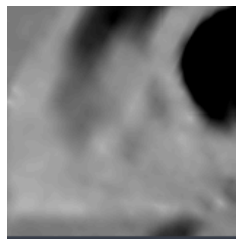

(b) Time frame 6

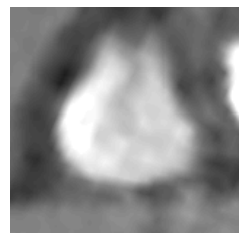

(c) Time frame 19

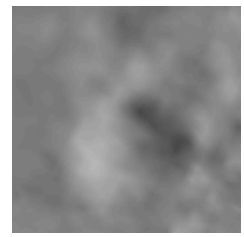

(d) Time frame 32

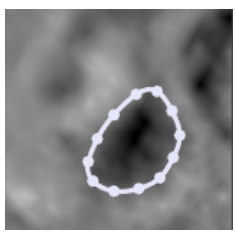

(e) Time frame 1

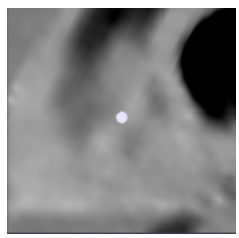

(f) Time frame 6

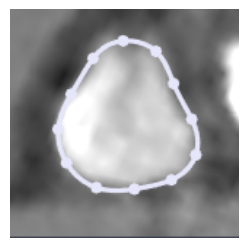

(g) Time frame 19

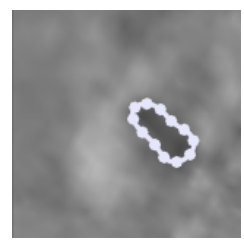

(h) Time frame 32

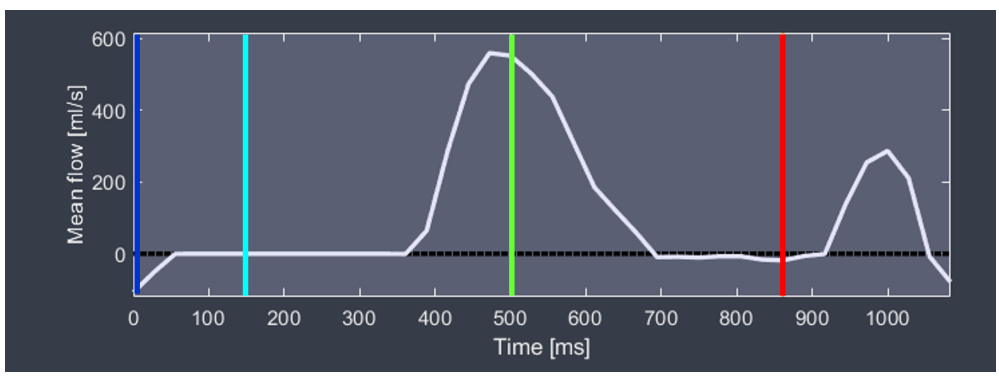

(i) Flow curve showing how the mean flow changes throughout the whole cardiac cycle. The coloured lines show time frames 1 (blue), 6 (cyan), 19 (green) and 32 (red).

Figure 5.5: Velocity images showing the tricuspid valve in four different time frames from a data set. The flow curve for the whole data set with the four time frames marked with coloured lines is seen in (i).

Velocity images from one data set showing flow through the tricuspid valve are found in Figure 5.5 where 5.5a-d shows unsegmented velocity images and 5.5e-h shows the automatically found ROIs. In time frame 1 a dark area was detected. A dip can be seen for this time frame in the flow curve in Figure 5.5i. In time frame 6 there is no flow of interest and the ROI has been reduced to a dot. Time frame 19 has the maximum mean flow which can be seen in the flow curve. The segmentation algorithm has captured the light area in Figure 5.5g. In time frame 32 a small dark area has been detected, this small area only results in a minor dip in the flow curve.

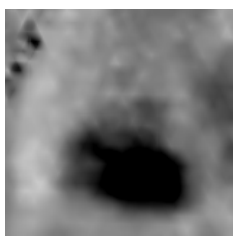

(a) Time frame 2

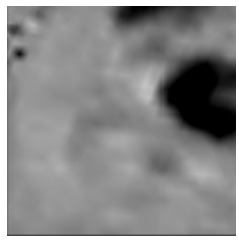

(b) Time frame 11

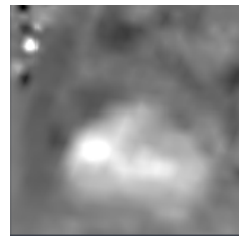

(c) Time frame 25

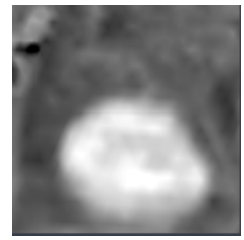

(d) Time frame 38

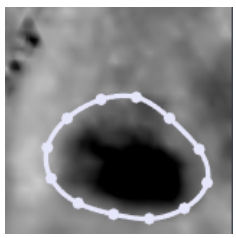

(e) Time frame 2

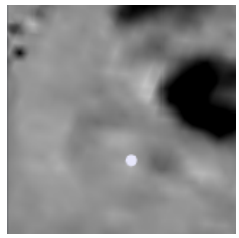

(f) Time frame 11

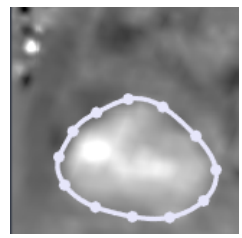

(g) Time frame 25

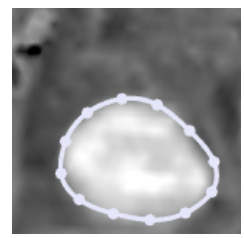

(h) Time frame 38

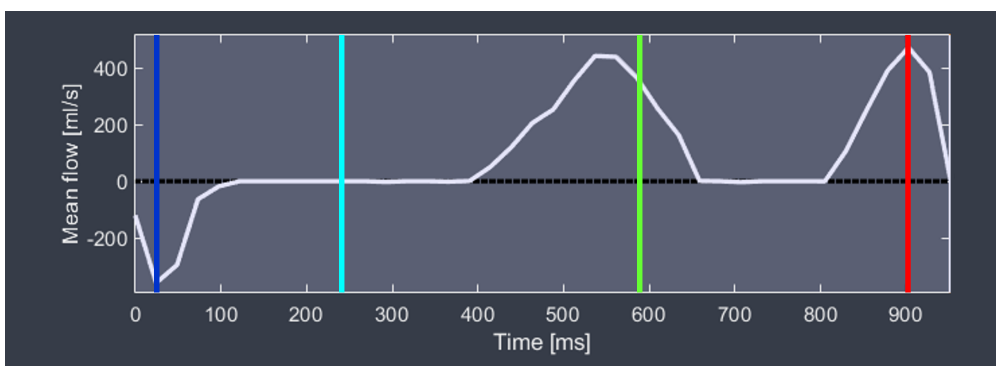

(i) Flow curve showing how the mean flow changes throughout the whole cardiac cycle. The coloured lines show time frames 2 (blue), 11 (cyan), 25 (green) and 38 (red).

Figure 5.6: Velocity images showing the tricuspid valve in four different time frames from a data set. The flow curve for the whole data set with the four time frames marked with coloured lines is seen in (i).

Velocity images for four time frames showing flow through the tricuspid valve are seen in Figure 5.6. The automatically found ROI are seen in Figure 5.6e-h and can be compared to the unsegmented velocity images in Figure 5.6a-d. In time frame 2 backflow has been detected and captured by the automatic segmentation algorithm setting the ROI. In the flow curve in Figure 5.6i there is a dip in the curve for this frame. In time frame 11 there is no flow, in time frames 25 and 38 valve flow has been detected.

5.3 Plane movement compensation

Figures 5.7 and 5.8 show how the volume measurements for one cardiac cycle for the mitral and tricuspid valves changed after plane velocity compensation.

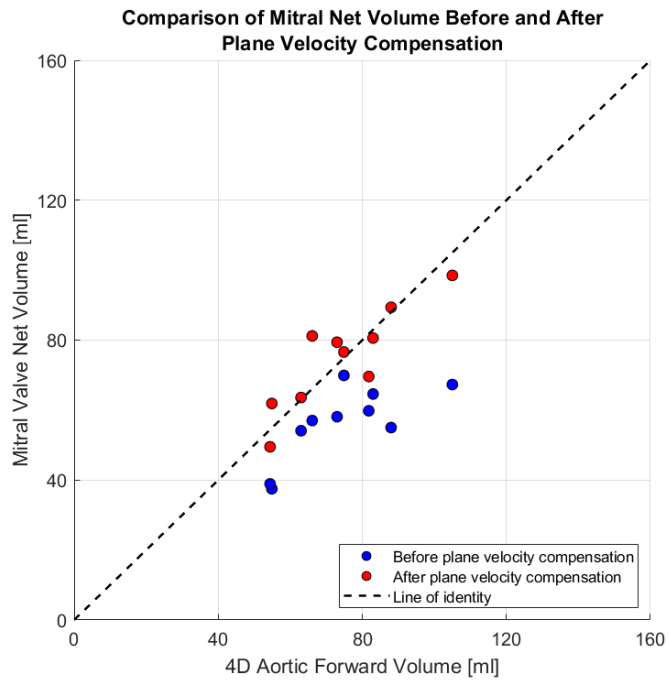

Figure 5.7: Comparing the mitral net volume with aortic forward volume in 4D before (blue) and after (red) compensation of the velocity of the moving mitral valve tracking plane. The comparison is made on a subset of the data from the heart failure patient group.

Figure 5.7 shows that the mitral volume measurements obtained after compensation of the plane velocity are closer to the line of identity than measurements before plane velocity compensation when comparing both to the 4D aortic volumes. The measurements before plane velocity compensation are located below the line of identity while the measurements after plane velocity compensation are distributed closer to and on both sides of the identity line.

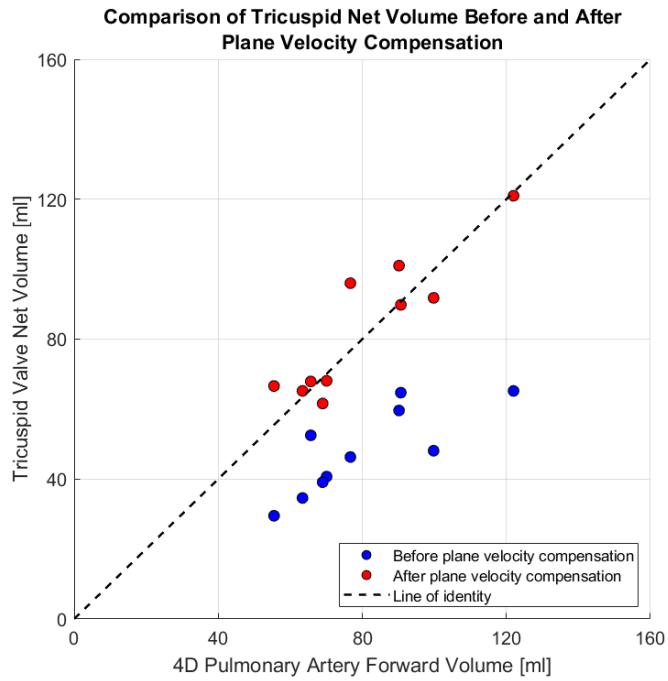

Figure 5.8: Comparing the tricuspid net volume with pulmonary forward volume in 4D before (blue) and after (red) compensation of the velocity of the moving tricuspid valve tracking plane. The comparison is made on a subset of the data from the heart failure patient group.

Figure 5.8 shows that when comparing the tricuspid valve volume measurements to the 4D pulmonary artery volume, the measurements obtained before the plane velocity compensation are located below the line of identity. The tricuspid volume measurements obtained after the plane velocity compensation are distributed closer and on both sides of the line of identity.

5.4 User interface and functions

Figure 5.10 shows how the 4D flow module looks after valve tracking has been completed. The valve tracking tool icon, see Figure 5.9, is found on the left side of the interface. The valve tracking planes appear in the 3-dimensional vessel tree model in the center. On the top right side of the interface an object list is found with the newly created mitral and tricuspid planes as well as 2CH and 4CH 2D images. The mitral valve object is selected and functions the can be run from the valve tracking plane are shown. In order left to right the functions are streamlines, pathlines, check alignment, regurgitation plane, edit plane size and gimbal (translation and rotation). Below the magnitude (left) and velocity image (right) of the plane is shown with the ROI. The ROI can be moved and resized with the buttons to the left of the images and the shape

of the ROI can be changed by dragging the ROI lines in the images. In the bottom right corner of the 4D flow module the flow measurements net flow, mean velocity, forward flow, maximum velocity and regurgitation fraction as well as the flow curves are shown for all flow measuring planes .

Figure 5.9: Icon for valve tracking

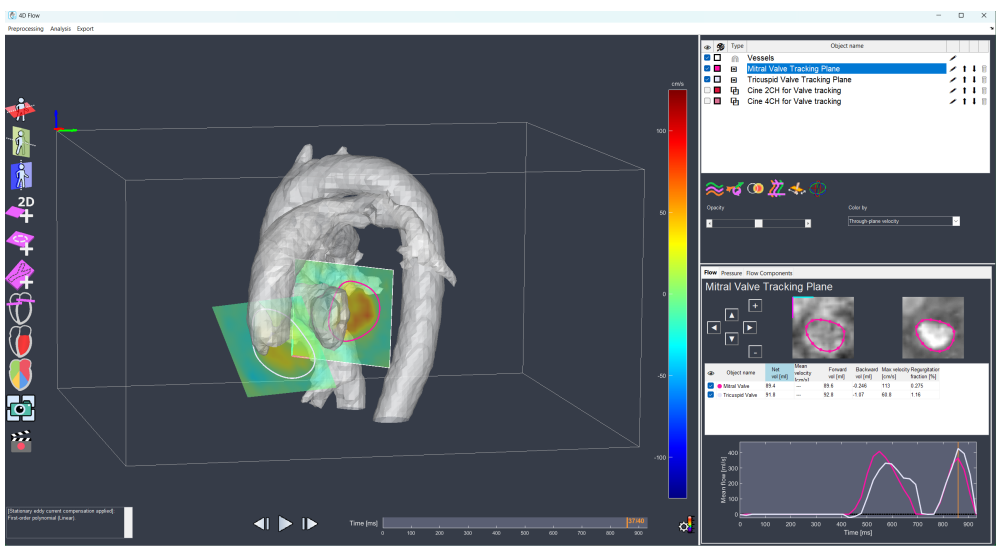

Figure 5.10: Segment 4D flow module after valve tracking has been completed.

Figures 5.11 and 5.12 shows a zoomed in view of Segment after the alignment check function has been run. In both images a 2CH cine image showing the anatomy is seen with a velocity map in colour showing the flow from the 4D data. By comparing the anatomical structures in the 2D cine image with the location of the flow it can be seen that the 2D and 4D data in Figure 5.11 is aligned, while it is unaligned in Figure 5.12.

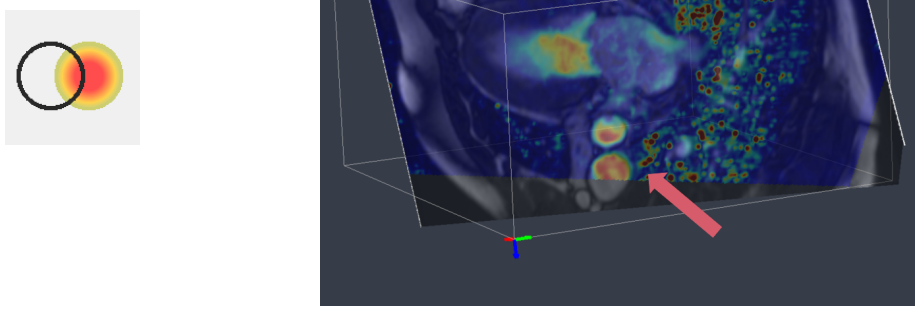

Figure 5.11: Image showing the alignment check feature on aligned data in the 4D flow module in Segment. Notice the alignment of the grayscale circles in the 2CH images at the bottom center of the images and the coloured circles (flow data).

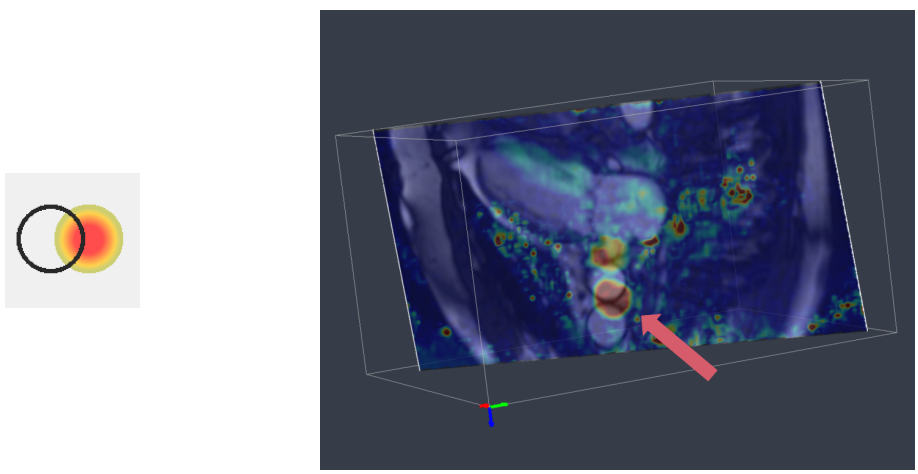

Figure 5.12: Image showing the alignment check feature on unaligned data in the 4D flow module in Segment. Notice the unalignment of the grayscale circles in the 2CH images at the bottom center of the images and the coloured circles (flow data).

Figure 5.13 shows the result of running the regurgitation plane function on a data set with tricuspid regurgitation. The icon for the function is shown to the left and a zoomed in view of Segment is shown to the right. The regurgitation plane is the top plane marked with a white line, and the background is a 4CH cine image. Streamlines showing the direction and magnitude of the flow are automatically activated for this function and can be seen between the regurgitation plane and the tricuspid plane. This is captured after the plane has been moved with the gimbal function (translation and rotation), which is also activated automatically.

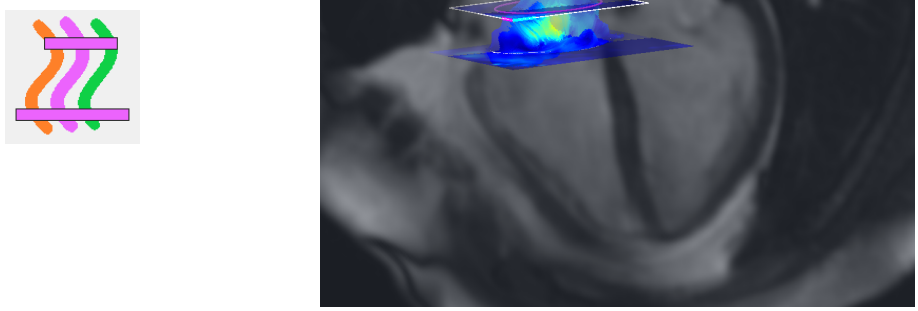

Figure 5.13: Image showing the regurgitation plane function on a data set with tricuspid regurgitation.

5.5 Validation

Two data sets were excluded for validation of the tricuspid valve tracking plane (1 healthy adult and 1 healthy child) due to difficulties in segmenting blood flow. The velocity images for these data sets did not have clear flows that could be segmented even manually. In Table 5.1 the number of data sets that needed some kind of manual corrections is presented. The adjustments include moving the valve tracking plane (translation only) due to the flow not being fully included in the original velocity image, corrections of ROI due to errors in segmentation and manual valve tracking for failed automatic valve tracking.

Table 5.1: Table showing the number of data sets that needed manual corrections.

Adjustment	**MV Siemens (corrected/n)**	**MV Philips (corrected/n)**	**TV Siemens (corrected/n)**	**TV Philips (corrected/n)**
Moved plane	1/37	-	2/35	1/7
ROI Correction	2/37	2/7	1/35	1/7
Manual valve tracking	-	-	2/35	-

The two data sets where automatic valve tracking of the tricuspid valve failed and manual tracking were needed were data sets of children. The semi-automatic valve tracking tool were used for these cases.

5.5.1 Mitral valve

The agreement between the mitral net volume and the 4D aortic forward volume is shown in the scatter and Bland-Altman plots of Figures 5.14 and 5.15.

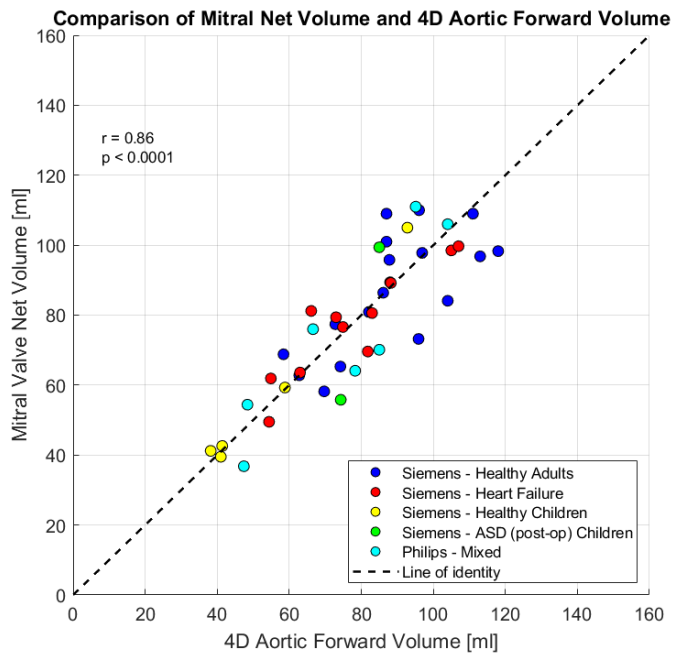

Figure 5.14: Scatter plot comparing the mitral net volume and 4D aortic forward volume measurements across different vendors and pathological groups.

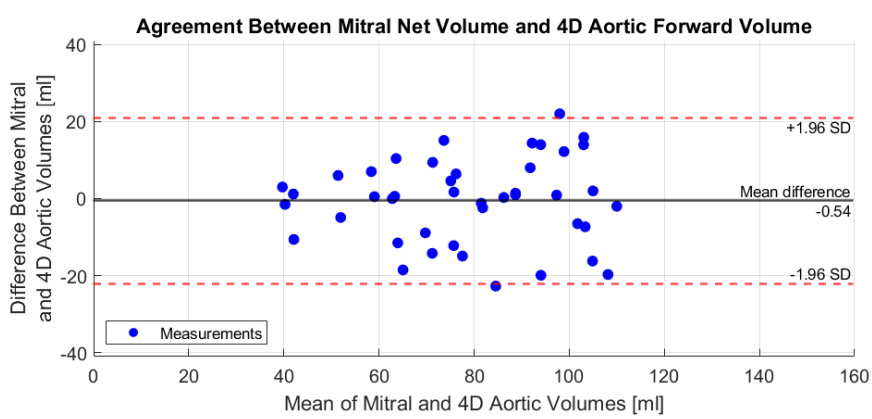

Figure 5.15: Bland-Altman plot showing the agreement between the mitral net volume and 4D aortic forward volume measurements.

In the scatter plot of Figure 5.14, the measurements from different vendors and pathological groups were distributed predominantly along the line of identity across the range of measurements. Lower measurement values were slightly closer to the line of identity compared to the intermediate and higher measurement values. The entire collection of mitral net volume measurements compared to 4D aortic forward volumes showed a correlation coefficient r = 0.86 and p-value < 0.0001. The Bland-Altman plot of Figure 5.15 shows that the majority of the measurements lie within the limits of agreement, with two outliers just outside the limits. The Bland-Altman analysis shows a mean difference of -0.54 ml between the mitral net volume and the 4D aortic forward volume.

The agreement between the mitral net volume and the 2D aortic forward volume is shown in the scatter and Bland-Altman plots of Figures 5.16 and 5.17.

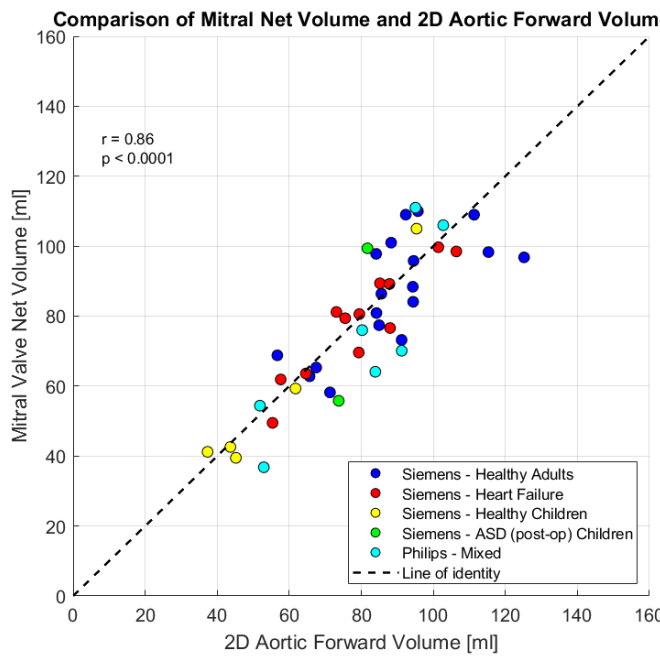

Figure 5.16: Scatter plot comparing the mitral net volume and 2D aortic forward volume measurements across different vendors and pathological groups.

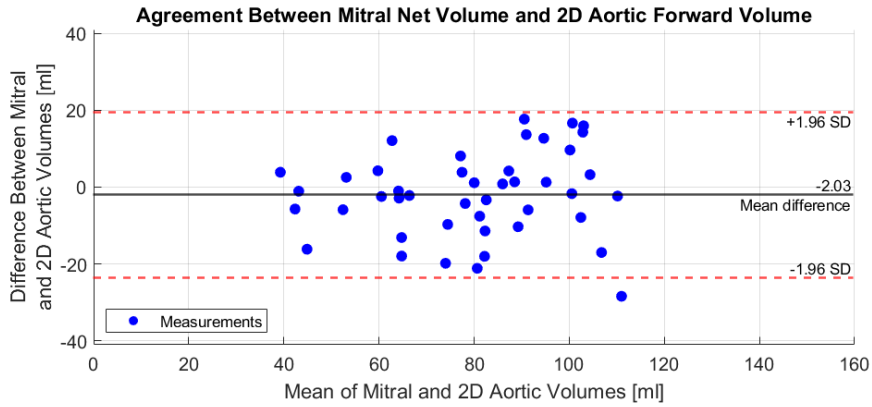

Figure 5.17: Bland-Altman plot showing the agreement between the mitral net volume and 2D aortic forward volume measurements.

In the scatter plot of Figure 5.16, the measurements from different vendors and pathological groups are mostly evenly spread within the same range along both sides of the line of identity. With the exception of one measurement for higher aortic volume, where the mitral volume measurement deviated further below the line of identity. The entire collection of mitral net volume measurements compared to 2D aortic forward volume has a correlation coefficient $r = 0.86$ and p-value < 0.0001. The Bland-Altman plot of Figure 5.17 shows that the majority of the measurement lie within the limits of agreement, except one outlier located below the lower limit. The Bland-Altman analysis shows that the mean difference between the mitral net volume and the 2D aortic forward volume measurements is -2.03 ml.

5.5.2 Tricuspid valve

The agreement between the tricuspid net volume and the 4D pulmonary artery forward volume is shown in the scatter and Bland-Altman plots of Figures 5.18 and 5.19.

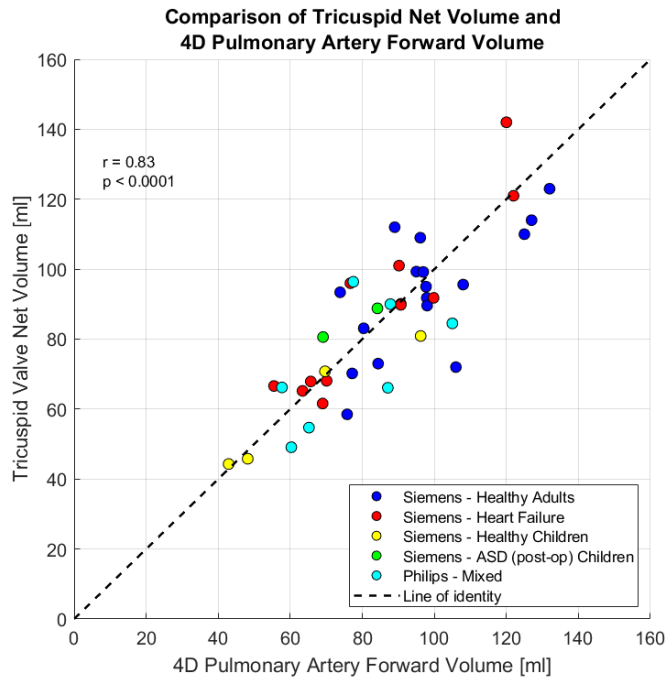

Figure 5.18: Scatter plot comparing the tricuspid net volume and 4D pulmonary artery forward volume measurements across different vendors and pathological groups.

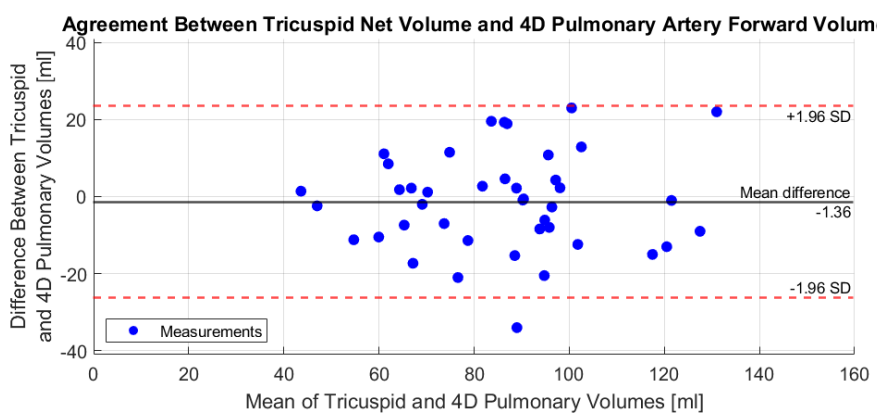

Figure 5.19: Bland-Altman plot showing the agreement between the tricuspid net volume and 4D pulmonary artery forward volume measurements.

The scatter plot comparing the tricuspid volume to the 4D pulmonary volume, in Figure 5.18, shows a dispersion on both sides of line of identity. The smaller cluster of higher measurement values looks to follow the dispersion of the bigger cluster. The tricuspid valve net volume measurements and the 4D pulmonary forward volume have a correlation coefficient r = 0.83 and p-value < 0.0001. The Bland-Altman analysis of the tricuspid and 4D pulmonary artery volumes in Figure 5.19 shows a mean difference of volumes between the tricuspid and 4D pulmonary artery measurement of -1.36 ml. The majority of the measurement points in the Bland-Altman analysis lie within the limits of agreement, apart from one outlier below the lower limit and one point on the upper limit.

The agreement between the tricuspid net volume and the 2D pulmonary artery forward volume is shown in the scatter and Bland-Altman plots of Figures 5.20 and 5.21.

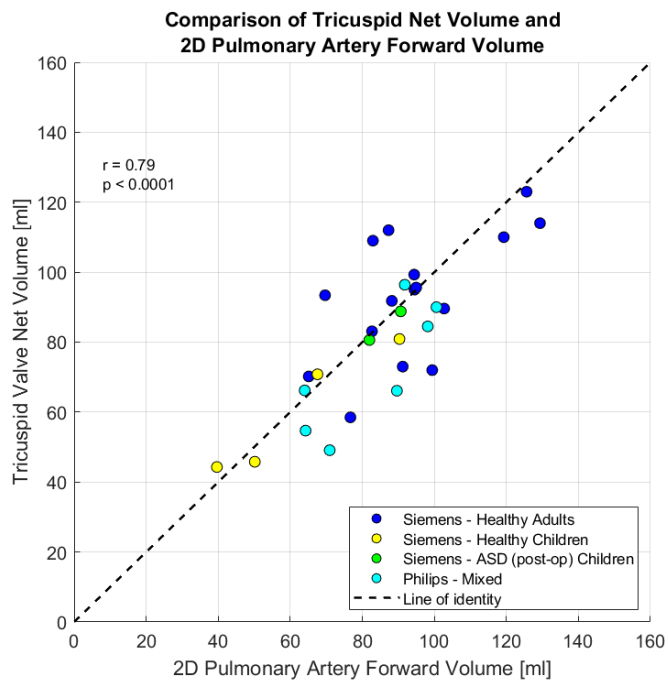

Figure 5.20: Scatter plot comparing the tricuspid net volume and 2D pulmonary artery forward volume measurements across different vendors and pathological groups.

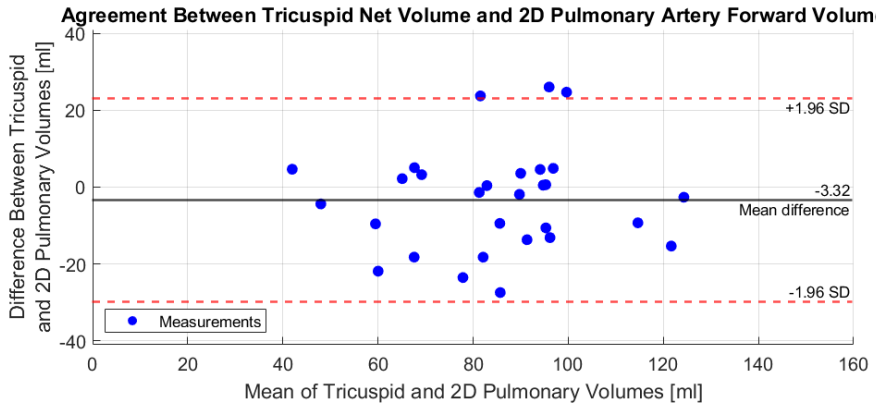

Figure 5.21: Bland-Altman plot showing the agreement between the tricuspid net volume and 2D pulmonary artery forward volume measurements.

The heart failure patient group from Siemens was excluded from the 2D comparisons including the pulmonary artery due to missing images to measure the pulmonary artery in 2D. In the scatter plot in Figure 5.20 the lower and higher measurement are close to the line of identity, while the larger cluster of intermediate measurements are more dispersed around the line. Between all the tricuspid valve net volume measurements and the 2D pulmonary forward volume the correlation has a correlation coefficient r = 0.79 and p-value < 0.0001. The Bland-Altman analysis in Figure 5.21 shows a mean difference of volume between the tricuspid and 2D pulmonary artery measurements of -3.32 ml. The majority of the measurement points in the Bland-Altman analysis lie within the limits of agreement, except for three outlier right above the upper limit.

5.5.3 Difference between volume measurements

In Table 5.2 the mean and standard deviation of the percentage difference is presented for different combinations of volume measurements. Measurements from the two different vendors are presented separately and together. The mean difference between each comparison is closer to zero for the Siemens data set (between -1.29% and 0.23%) than for the Philips data sets (between -12.56% and -1.84%).

Table 5.2: Table of mean and standard deviation of percentage difference between pairwise volume measurement comparisons across different vendors and in total. Number of data sets (n) are reported as Siemens/Philips/Total.

	Siemens	**Philips**	**Total**
Mitral / Aorta 4D (%) [n = 36 / 7 / 43]	0.23±12.78	-1.84±17.07	-0.10±13.35
Mitral / Aorta 2D (%) [n = 37 / 7 / 44]	-1.19±12.18	-8.24±17.76	-2.31±13.23
Tricuspid / Pulmonary 4D (%) [n = 35 / 7 / 42]	0.12±13.58	-5.25±19.10	-0.78±14.50
Tricuspid / Pulmonary 2D (%) [n = 22 / 7 / 29]	0.02±16.18	-12.56±13.52	-3.02±16.29

5.5.4 Difference between volume measurements in Segment and Caas

Table 5.3: Table of percentage difference between valve net volume measurement (ml) in Caas MR 4D Flow and Segment 4D Flow.

Mitral (Segment)	**Mitral (Caas)**	**Difference (%)**	**Tricuspid (Segment)**	**Tricuspid (Caas)**	**Difference (%)**
69.6	70.5	-1.28	67.9	70.4	-3.55
80.9	78.24	3.40	83.1	86.94	-4.42
62.8	64.4	-2.48	93.4	76.6	21.93
110	104.19	5.58	99.2	96.58	2.71
54.4	53.3	2.06	66.2	66.17	0.05
70.1	85.85	-18.35	96.4	93.22	3.41
103	110.36	-6.67	114	110.52	3.15
98.5	81.9	20.27	101	73.6	37.23

In Table 5.3 the percentage difference of net volume measurements in Segment 4D Flow and Caas MR 4D Flow for the mitral and tricuspid valves are presented. With the exception of three data sets, the difference between valve volume measurements in Segment 4D flow and Caas 4D flow ranges between -6.67% to 5.58%.

In the data set where the volume measurements of the tricuspid valve differs 21.93% between the two systems, the data and velocity images of the tricuspid valve plane were abnormal making it difficult to segment the flow in Segment. The velocity image in Caas looked different which may be due to it not being located in exactly the same place as in Segment or due to how it is displayed in Caas in terms of contrast and size. This resulted in differences to how the ROI was decided. The tricuspid valve measurement obtained in Caas produced a value more in line with the pulmonary artery measurements from Segment as well as with the mitral and aortic values of the same case. For the data set where the mitral volume measurements differs -18.35%, the volume measurement from Segment for the valve were unexpectedly low when comparing it to the aorta flow in Segment. In this specific case it seems like the valve tracking produces points that moves in an unusual pattern causing the plane velocity compensation to fail to properly adjust the flow. The manual tracking in Caas produced a result more in line with the other measurements for this case. In one data set the mitral valve volumes differed 20.27%, as well as the tricuspid volumes with a difference of 37.23%. In this case the aorta volume was difficult to measure in 4D due to vortices. The aorta volume from the 2D image was found to be 106.39 ml in Segment and 100.32 in Caas, the difference likely due to some differences in vessel segmentation. When comparing the volume in the mitral valve found in Segment (98.5 ml) and in Caas (81.9 ml), the value from Segment is more in line with the aorta volume. No data was available to measure the pulmonary artery volume in 2D, however the volume in the pulmonary artery is expected to be close to, or even a few millilitres higher, than the aortic volume. Comparing the tricuspid volume measured in Segment (101 ml) and in Caas (73.6 ml), the value from Segment is closer to the expected volume.

In Table 5.4 the time to run the valve tracking tool for Segment and Caas is presented as well as the difference. The tools works differently where valve tracking in Segment is fully automatic, whereas in Caas the valve tracking is semi-automatic and the flow segmentation has to be done manually meaning that everything is checked along the way by the user. Therefore both the run time and a time to check the results are included for the time in Segment to make the comparison more fair.

Table 5.4: Table of run time of the valve tracking tool in Segment 4D flow and in Caas MR 4D Flow

	Segment (runtime + check)	**Caas**	**Difference**
	12s + 40s	7min	6min 8s
	10s + 50s	5min 20s	4min 20s
	16s + 20s	3min 50s	3min 14s
	13s + 25s	8min 20s	7min 42s
Average:	**46.5s**	**6min 7s**	**5min 21s**

6

Discussion

The scatter plots comparing mitral–aortic and tricuspid–pulmonary volumes for one cardiac cycle, before and after plane velocity compensation, show that valve volume measurements before plane velocity compensation are below the line of identity. Volume measurements after plane velocity compensation are distributed closer to and around the line of identity, concluding that plane velocity compensation is needed for more accurate measurements. With the plane velocity compensation the blood volume that passes through the plane as it moves is accounted for. Without plane velocity compensation this volume is missed, resulting in a systematic underestimation of flow.

The validation of the method for mitral valve flow quantification demonstrates strong correlations when comparing volumes for one cardiac cycle for the mitral valve and the aorta in both 4D and 2D ($r = 0.86$ and $p < 0.0001$ for both comparisons, Figures 5.14 and 5.16). The comparisons between mitral and aortic volume show a linear trend, where higher aortic volume corresponds to higher mitral volume. The Bland-Altman analyses showed a small negative bias for the comparison between the mitral and 4D aorta volumes (-0.54 ml, Figure 5.15) and 2D aortic volume (-2.03 ml, Figure 5.17), indicating a slight underestimation of the mitral volume compared to the aortic volume. The limits of agreement in the comparisons between mitral and aortic volumes are indicating a variability where individual measurements can differ.

The validation of the method for tricuspid flow quantification shows a strong correlation and low bias. The correlation between the tricuspid volume and the 4D pulmonary volume is slightly stronger ($r = 0.83$, $p < 0.0001$, Figure 5.18) than between the tricuspid volume and the 2D pulmonary artery volume ($r = 0.79$, $p < 0.0001$, Figure 5.20). However it is important to note that the comparison with 2D pulmonary included less data points as the heart patient group was excluded, due to the data sets missing images for 2D pulmonary measurements. The Bland-Altman analyses of the tricuspid volume measurements show a low negative bias indicating a slight underestimation of the tricuspid valve volumes. For tricuspid and 2D pulmonary volume the bias is deviating a bit more (-3.32 ml, Figure 5.21) than for tricuspid and 4D pulmonary

volume (-1.36 ml, Figure 5.19). The variability between individual measurements is shown by the limits of agreement.

While the biases of the comparisons are low, the Bland-Altman analyses and Table 5.4 showing the standard deviations of the measured volumes demonstrate a relativity large variability in the individual volume measurements. The volumes in the valves and the aorta and pulmonary artery are expected to be about the same. The volume in the aorta should be about 5% less than the volume in the pulmonary artery. When looking at the agreement between the two in Figures 4.11 (4D/4D) and 4.12 (2D/2D) the differences are -5.92 ml and -4.21 ml respectively which is explained by the expected 5% difference. However the limits of agreement are wider for the 4D comparison, where the measurements indicate a larger individual variety than the 2D data. This variety is also seen for the valve volume measurements, which are calculated from 4D data, when comparing them to measurements from 4D and 2D data. This indicates that variations in 4D data may be a common issue. Therefore, the variability observed during the validation of the valve flow quantification method may not necessarily reflect the performance of the method itself, but could instead be influenced by variability and inconsistencies within the 4D flow data. Imaging settings like temporal and spatial resolution as well as VENC can influence the results. Aliasing caused by a too low VENC can cause errors and inaccurate results. Another source for variations can be complex flow patterns at the mitral and tricuspid valves, where the flow can be turbulent with vortices. Vortices can also be found in the aorta and pulmonary artery making it more difficult to find an appropriate place to measure flow. Vortices can cause errors in measurements and while different locations to measure flow can be tested in the aorta and pulmonary artery this is not an option for the valves. Flow measurements may be less precise for turbulent flow, due to the phase contrast images being optimized for laminar flow [20]. Furthermore the large variability could also be caused by the greater technical complexity of the mitral and tricuspid flow quantification methods. The valve flow quantification methods include valve tracking, flow segmentation and plane motion compensation, each adding variables that can affect the flow measurements.

The mean differences were larger for the Philips data sets compared to Siemens and also demonstrated slightly larger variability, see Table 5.2. The number of Philips data sets were 7, compared to 37 Siemens data sets. While the results suggest more unreliable results for Philips data, further investigation is needed with more data before any conclusions can be drawn.

The comparisons between the valve volume measurements made with the implemented valve tracking in Segment 4D flow and the already available valve tracking in Caas MR 4D flow, shown in Table 5.3, show that the solutions seem to be comparable. There are some differences in the measurements which may be due in how the two programs preprocesses and handles aliasing and other artefacts in the different data sets.

Both programs additionally compensate for plane velocity, and potential differences in how this compensation is calculated may also contribute to the observed differences. Furthermore, the differences may also be due to differences in segmentation. In Caas, the initial ROI placed by the software is static and the ROI is then needed to be manually adjusted in each time frame to segment the correct flow. Whereas in Segment the interesting flow is automatically segmented in each time frame, and the ROI only needs to be manually corrected in certain time frames. The possibility to manual correct the segmentation is important to adjust any incorrect segmentations as even small changes sometimes can noticeably impact the result. The need to manually adjust the segmentation and the semi-automatic valve tracking in Caas is the reason why the run time of valve tracking in Caas is on average 6 minutes and 7 seconds, see Table 5.4. Where in contrast, the fully automatic valve tracking in Segment on average takes 46.5 seconds, which includes the time it takes to check the results. Three data sets had large differences, two for the mitral valve and two for the tricuspid valve. Two of these data sets, one mitral and one tricuspid, had internal inconsistencies within the volume measurements in Segment. The volume in the tricuspid valve was higher than expected, where the velocity image was difficult to segment in Segment. The image looked different in Caas, resulting in a different segmentation of the flow. Differences in how the velocity images are displayed as well as the placement of the plane can be causes of these perceived differences and can in the end impact the results. The low value for the mitral valve seemed to be due to issues with the plane compensation most likely caused by abnormal movement of the plane from the valve tracking. The results in Caas were more in line with what was expected. In one data set the volume in the mitral valve and the tricuspid valve from Segment was more in line with the 2D data from both systems. The issue here may have had something to do with the plane compensation in Caas as the values before any compensation was made were similar to the values in Segment without compensation. This shows that valve tracking and possible differences in plane movement compensation between the systems can be cause discrepancies.

6.1 Automatic valve tracking

In this project the already implemented valve tracking networks MVnet and TVnet were used. Another network was tested that had been trained to find points for the mitral and tricuspid valves in the EDT time frame. This network failed in identifying points in all time frames in an unacceptable amount of data sets and therefore MVnet and TVnet were tested instead and they proved more successful. Both MVnet and TVnet uses two networks where the first finds an approximate location of the valve points and the second a more precise location. These more complex and larger networks were needed for accurate tracking, but the tracking process takes some time which is unavoidable. Efforts were made however to cut down run-time to improve user experience by ensuring the networks only have to be loaded the first time after Segment has been started. If the tracking has been completed for a data set this will

also be recognized and it will not run again. Wait bars were added for these processes to inform the user of what is happening and the progress.

In 2 out of 7 data sets of children examined, the automatic valve tracking of the tricuspid valve predicted the location of the valve incorrectly, see Table 5.1. This could be due to the training of TVnet not being as extensive as the training of MVnet, as TVnet is trained on data sets from 140 patients scanned on Siemens scanners whereas MVnet is trained on data from 703 patients, including children, from scanners from different vendors. If the automatic tracking fails, the already implemented tool for semi-automatic tracking can be used instead in Segment. With the modifications made for it's output, the tool from this project in the 4D flow module will recognize if this tracking tool has been used to allow the user to use those points instead. In case only small adjustments are needed it is also possible to move the automatically detected valve points in individual time frames. These possibilities ensures that the tool created in this project is still able to measure valve flow from 4D data even if the automatic valve tracking fails or needs adjustments.

6.2 Creation of planes

In this project valve points are automatically detected in standard left ventricle 2CH and 4CH MR-image views. The use of these standard image view makes the tool more accessible since no special images are needed. This can make the tool especially useful for research purposes when already collected data is used where standard view most likely will be included. It is also useful clinically since no special imaging protocols to collect specific image view are needed, only the standard views. For the purpose of creating planes for the mitral and tricuspid valves it would however naturally be better to have two orthogonal views of each valve to completely capture the size and angle of the plane in the 3D space. The angle of the mitral valve can be derived from the 2CH and 4CH images since four points are found, but the size had to be approximated. For the tricuspid valve the size also had to be approximated. Different sizes were tested for for both valves on a multitude of data sets to find an appropriate size that will include the whole valve but not be large enough to include much of flow in the surrounding area. An appropriate size was found for both that works well on the majority of data sets. The tricuspid valve plane was set to be bigger than the mitral valve plane since it is generally larger. A function for changing the size of the plane was added in Segment for the valve tracking planes to let the user edit the size in case it is needed. The location of the tricuspid plane was also adjusted since placing the plane with the center aligned to the 4CH image resulted in flow being missed. The plane was moved in the anterior direction.

For the tricuspid the angle had to be approximated since points are only found in the 4CH image. To define a plane at least 3 points or a directional reference is needed. To be able to create a tricuspid plane the tilt of the plane needed to be approximated

and the angle of the mitral valve was chosen as a starting point. Since no exact angle in relation to the mitral valve could be found in any literature the angle was found through testing. The tricuspid plane ended up with a slight tilt in relation to the mitral plane, but as previously stated in 4.2.2 the changes in angle did not make a drastic change in the final measurements. It was however a slight improvement and since anatomical models seems to show some difference in angle this found angle was used. This does however introduce some uncertainty in regards to the results of the flow through the tricuspid valve. Since the flow is measured from the velocities perpendicular through the plane, an incorrect tilt of the plane can cause incorrect measurements. The anatomical relationship between the mitral and tricuspid valve can also vary between patients. Using a set angle of the tricuspid valve based on the mitral valve orientation can therefore cause the tricuspid valve plane to be incorrectly tilted. Ideally the plane should be orthogonal to the flow, although a $\pm 15^{\circ}$ deviation is acceptable meaning that there is some margins. A function for moving and tilting the plane in three directions (referred to as the gimbal function) was added for the valve tracking plane to allow for adjustments if needed.

Improvements that could be made is to include the opportunity to use other image views. Right now the automatic valve tracking is confined to using left ventricle 2CH and 4CH images. Right ventricle 2CH images could be tested to see if the prediction would work on them as well, if not a network could be trained to track the tricuspid in them as well. A network that can automatically track points in a 3CH image could also be considered, although that would only provide one point more for the tricuspid but that would be enough to get a directional reference.

6.3 Automatic flow segmentation

Two different flow segmentation algorithms had to be written, one for the mitral valve and one for the tricuspid valve. The algorithms share a common structure, but each needed some different methods and adjustments. For the segmentation of positive and negative flow of the mitral valve plane as well as for the negative flow of the tricuspid valve plane, a global threshold was used to identify the flow in each frame. One could think that only the largest positive or negative flow velocity area each time frame would be needed to determine the threshold of each time frame. However due to the velocities differing quite a lot between time frames and where some images did not have any flow of interest, a global threshold is needed to identify what is actually identified as interesting flow in each time frame. The local threshold was still calculated and compared with the global threshold. If the local threshold was closer to zero than the global threshold, indicating large gray areas with no interesting flow, the local threshold was used to avoid including the gray areas. While this approach was tested for segmenting the positive flow in the tricuspid valve, it did not work as some time frames had large light areas that were not valve flow that were mistaken for such. As this problem only was found for the tricuspid valve it could be due to some

differences in anatomy that this occurs. To overcome this issue, the maximum positive velocity in the data set was identified and a mask was created of the segmented area in that time frame that was then used for all frames. The downside of this approach is that this time frame may not capture the maximum area of positive valve flow. The mask was dilated slightly to account for this.

One of the main challenges during the automatic segmentation was to find suitable thresholds that performs well on all data sets. As seen in the Figures 5.2-5.6 the velocity image of the valve tracking plane vary quite a lot in intensity and noisiness between different data set. These differences create challenges during segmentation as one threshold may work well for some data set, while failing to correctly segment other data sets where the velocity images are different. The final thresholds were found through testing different thresholds on a large number of data sets with varying velocity images, and the thresholds performing well on the data sets were chosen.

In time frames where no interesting flow was found the mask of the ROI was set to a point. This was important to do, since even though there was no interesting flow to measure, as the background and positive flow mask are similar, there might still be some slight offsets from zero in the velocities within the mask. Measuring these small velocities as flow within the mask over several time frames, when there is no interesting flow to measure, will accumulate flow that can bias the total flow measurement. Setting the mask of the ROI to a point was therefore necessary to avoid adding bias to the flow measurements. However, this is not implemented in the already existing static planes used for measuring the flow in the aorta and pulmonary artery. In the static flow measuring planes, the ROI is initialized as a circle for all time frames. As correcting the ROI to be a point in every time frame where no interesting flow is present in the aorta or pulmonary artery would be very time consuming, this correction was not made for the measurements of the aortic and pulmonary artery. By not excluding the unwanted irrelevant velocities a bias may have been added to each aortic and pulmonary artery measurement.

When defining the final mask and determining what negative flow should be considered regurgitation or other flow to exude, checking the overlap of each negative velocity object with the positive velocity mask is crucial. Checking if the centroid of the object overlaps with the positive velocity map, ensures that this negative flow is considered to be inside of what considered to be the valve. If there is no interesting forward flow, while there is negative flow within the area considered as the valve, this flow is masked and included as potential regurgitation. For the mitral valve segmentation the maximum area of the aorta in all time frames was found. A mask was created of this area and potential overlap of all negative flow objects were checked with this aorta mask. If overlap was found, the object was identified as aorta flow and therefore removed. This was needed since the areas where aorta and mitral valve flows are found overlaps, requiring a solution to correctly separate regurgitation and aorta flow as the

can occur in the same time frame as demonstrated in Figure 5.3.

The final number of points visible in the graphical interface were chosen to be 12. This number was needed to capture the varying shapes of the valve flow. A negative side effect of that many points is that correction of the ROI in the 4D flow module can become time consuming if the whole ROI needs to be changed in a specific time frame as more points need to be moved. It does of course also provide the opportunity to more precisely control the shape of the ROI. An improvement that can be made is to allow the user to use the buttons for moving and changing size of the ROI for only one time frame. A change using these buttons will now result in a change in the ROI in all time frames leaving only the option of dragging the ROI points in the velocity image for individual alterations. A smoothing filter was applied in the spatial direction to ensure that the ROI does not completely change shapes in between time frames. Without this filtering the ROI would be more prone to accidentally include artifacts. It is not expected that the shape changes that much in between time frames, more so that it changes size. Quick updates are needed between time frames, which is why such a filter was not applied in the temporal direction.

Although the segmentation is satisfactory in most cases, having the possibility for the user to make manual corrections to the ROI provides more robustness in the cases where segmentation does not perform as wanted. Of out 44 data sets where mitral volume was measured, 4 needed manual correction of the ROI due to distinct errors in the segmentation and thereby the volume measurements, see Table 5.1. For the 42 tested data sets for tricuspid volume 2 needed correction. This shows that the segmentation algorithm works well to automatically detect flow. For some data sets it can be difficult to identify the flow as the colours may be blended and the edges unclear. It can also be unclear if some areas are actually flow, or an image artefact. It was noticed that for some data sets small changes to the ROI could result in a relatively large change to the end results, while for some it did not. The automatic segmentation should be used a base but the the velocity images in the whole data set should be checked to asses the quality of the data and the segmentation should be checked as well to ensure that it is acceptable.

6.4 Alignment

The limiting factor for introducing the automatic alignment algorithm was the variety and quality of the data. It was difficult to create image processing functions to create the masks due to large varieties in intensity values and contrast in the magnitude images. Settings that worked well for one dataset could fail for other data. Artefacts and patient movement during imaging also results in bad quality images that is difficult to segment and then match. Further work has to be done and other methods should be investigated for an automatic alignment tool, unfortunately the time limit of this project did not allow for taking on this task.

A tool to check alignment was created and the view after it has been run in Segment is seen in Figures 5.11 and 5.12. This tool is intended to provide an easy way to check for misaligned data, as that is a fairly common source of error when working with combined 2D and 4D data. A future tool that could be added is a manual alignment tool in the 4D flow module in Segment, where the user after checking that alignment is needed could choose the tool to align the data. In this manual alignment tool the user could have the ability move the 2D images of the 2CH and 4CH view that appear with the alignment check tool to align the image with the corresponding velocity map of each image. The movement of the images could be done with buttons for up, down, left and right and when pushing a button the image is move a certain increment in that direction. The movement would then change the position of the 2D images.

6.5 Graphical interface and functions

During the implementation of the valve tracking tool into Segment's 4D flow module the user experience was considered. Wait bars were added for the processes that could take some time like loading the networks and updating the graphical interface. The colour bar was also changed so that both positive and negative flows could be visualized in the planes in the 3D space. Before the scale was from zero to the maximum positive velocity limit meaning that only flow in one direction was visible in the planes. Figure 5.11 shows this colour scheme where background (zero velocity) is blue with positive flow showing in red. This can be compared with the planes in Figure 5.10 where the planes are green and where negative flow will be shown as blue and positive flow as red. This adjustment was needed as the valve tracking planes should show both flow through the valve as well as eventual backflow.

The decision to automatically create objects to visualize the 2CH and 4CH were made to make it easier to check how the automatic valve tracking performed. Adding 2D images is already a feature in Segment's 4D module so this could have been left to the user to do manually. Since the performance of the tracking algorithm is essential it was decided to include this automatically since that would be a common thing the user checks.

Each object type in the module has it's own functions and tools connected to it. The icons for them can be seen in Figure 5.10 under the object list in the top right. Which tools to include for a valve tracking plane was considered and it was decided that streamlines and pathlines should be included to be able to visualize flow. As was discussed in Section 6.2 the size of the planes as well as the angle of the tricuspid plane had to be approximated. Therefore a function to edit the size of the plane as well as a way to move and rotate the plane (gimbal function) was added. The set size of the planes was found to work well, but in a few cases small adjustments were

needed which is easy to do with the size adjustment tool. If the 2D and 4D data is slightly unaligned, resulting in some flow not being included in the area of the plane, the gimbal is an easy way to adjust the position of the plane to move it so that the flow of interest is in the center. It can also be used to test different rotations of the planes. All of these functions were already implemented in Segment for other types of planes, although they all had to be altered since they were made for static planes and the valve tracking plane moves. Two new functions were also made, one for an easy way to check alignment as discussed in Section 6.4 and a function to place a regurgitation plane. The importance of measuring regurgitation some distance away from the valve where flow is more coherent was discussed by Blanken et al. in [24]. A plane to measure flow can be created by the user in Segment by choosing that tool and then clicking on the surface of the vessel tree. It was found that the left and right atrium was not included in the vessel tree in the 4D module, meaning that a plane could not simply be placed there. A plane could be created somewhere else and then moved to location of the regurgitation with the gimbal function and then possibly also be resized to include the correct flow. As this was time consuming it was decided to create a function that will use the position of the valve tracking plane to place a smaller plane above it. The decision to automatically include streamlines in the regurgitation function was made since a guide of where to move the plane was needed. The plane will not automatically be placed correctly, the user need to identify the flow of interest from the streamlines and move the plane. To signal that the user is expected to move the plane into location, as well as to reduce the number of clicks, the gimbal function is automatically activated.

6.6 Ethical Considerations

All data used in this project has been collected with informed consent from test subjects and patients for research purposes. Prior to usage all data was pseudonymized to protect patient information.

Before the valve tracking tool is used for research or in clinic, thorough and extensive testing and validation need to be performed. Segment is intended to be used as a complementing tool in clinic for assessment of patients. The output of the diagnostic tool should not be interpreted in isolation. Instead, healthcare professionals are expected to consider the results together with other relevant clinical information when making decisions. With the release of the software researchers and clinicians are expected to critically evaluate the results, exercise independent judgment, and report any problems.

7

Conclusion

While the validation of the mitral and tricuspid flow quantification method show high correlation and low biases, the method have an unexpectedly large variability between individual measurements. This could also be seen for the comparison between aorta and pulmonary artery volumes from the 4D data. The relatively high variability in the 4D data makes validation challenging and may affect the reliability of the measurements. This suggests that the variability observed during the validation is not necessarily a reflection of the performance of the proposed valve flow quantification method, but could be due to uncertainties within the 4D flow data. It should also be noted that the proposed valve flow quantification method relies on multiple processing steps, including valve tracking, plane movement compensation, and flow segmentation, each of which may introduce additional uncertainty into the measurements. These initial results do however suggest that the proposed method is promising, with valve tracking performing well in the majority of cases, although failures were observed in a small number of pediatric datasets involving the tricuspid valve. The automatic segmentation also showed generally robust performance across most cases. Overall, the results obtained with the proposed method were largely comparable to those from Caas, with remaining differences likely attributable to factors such as differences in preprocessing, segmentation, and plane movement compensation. An important advantage of the proposed method compared to Caas is its automated workflow and substantially shorter analysis time. Considerations for usability and user experience were made for the valve tracking tool in Segment where opportunities for manual adjustments were included. Functions for checking 2D/4D data alignment and creating a plane to measure regurgitation were implemented to facilitate faster and easier analysis of the data.

Further investigation of the characteristics and limitations of the 4D flow data is needed, together with a more comprehensive evaluation of the newly implemented valve flow quantification method in Segment. The present results demonstrate encouraging performance, but also highlight sources of variability that require further analysis.

Bibliography

[1] A. Taylor, S. Dymarkowski, and J. Bogaert, "Valvular Heart Disease," in *Clinical Cardiac MRI*, ser. Medical Radiology, J. Bogaert, S. Dymarkowski, A. Taylor, and V. Muthurangu, Eds., Berlin, Heidelberg: Springer, 2011. DOI: 10.1007/174_2011_414.

[2] A. Weinhaus, "Anatomy of the Human Heart," in *Handbook of Cardiac Anatomy, Physiology, and Devices*, P. Iaizzo, Ed., Cham: Springer, 2024. DOI: 10.1007/978-3-031-72581-4_4.

[3] Y. Wapcaplet, *Diagram of the human heart (cropped)*, Wikimedia Commons, Licensed under CC BY-SA 3.0, 2026. [Online]. Available: https://commons.wikimedia.org/w/index.php?curid=830246.

[4] J. Zhingre Sanchez, M. Bateman, J. Quill, A. Hill, and P. Iaizzo, "The Anatomy and Function of the Atrioventricular Valves," in *Heart Valves*, P. Iaizzo, T. Iles, M. Griselli, and J. St. Louis, Eds., Cham: Springer, 2023. DOI: 10.1007/978-3-031-25541-0_1.

[5] L. Crumbie, *Heart valves*, 2023. [Online]. Available: https://www.kenhub.com/en/library/anatomy/heart-valves.

[6] Wikimedia Commons contributors, *2011 heart valves*, Wikimedia Commons, Retrieved 24 March 2026, 2023. [Online]. Available: https://commons.wikimedia.org/w/index.php?title=File:2011_Heart_Valves.jpg&oldid=750885430.

[7] C. Gopalan and E. Kirk, "The Heart," in *Biology of Cardiovascular and Metabolic Diseases*, Elsevier, 2022, pp. 1–33. DOI: 10.1016/B978-0-12-823421-1.00011-1.

[8] W. A. Zoghbi et al., "Recommendations for Noninvasive Evaluation of Native Valvular Regurgitation: A Report from the American Society of Echocardiography Developed in Collaboration with the Society for Cardiovascular Magnetic Resonance," *Journal of the American Society of Echocardiography*, vol. 30, no. 4, pp. 303–371, 2017. DOI: 10.1016/j.echo.2017.01.007.

[9] R. John and C. Siems, "Heart valve disease," in *Heart Valves*, P. Iaizzo, T. Iles, M. Griselli, and J. St. Louis, Eds., Cham: Springer, 2023. DOI: 10.1007/978-3-031-25541-0_4.

[10] Internetmedicin, *Mitralisinsufficiens – utredning*, Internetmedicin, Retrieved 25 March 2026, 2026. [Online]. Available: https://www.internetmedicin.se/kardiologi/mitralisinsufficiens#utredning.

[11] D. Weishaupt, V. D. Koechli, and B. Marincek, *How does MRI work?: An introduction to the physics and function of Magnetic Resonance Imaging*. Springer Berlin / Heidelberg, 2008.

[12] V. Muthurangu and S. Dymarkowski, "Cardiac MRI Physics," in *Clinical Cardiac MRI*, ser. Medical Radiology, J. Bogaert, S. Dymarkowski, A. Taylor, and V. Muthurangu, Eds., Berlin, Heidelberg: Springer, 2011. DOI: 10.1007/174_2011_412.

[13] S. Azhar and L. R. Chong, "Clinician's guide to the basic principles of MRI," *Postgraduate Medical Journal*, vol. 99, no. 1174, pp. 894–903, Aug. 2023. DOI: 10.1136/pmj-2022-141998.

[14] W. Y. Tseng, Y. H. Tseng, and M. Y. Su, "Introduction to Cardiovascular Magnetic Resonance: Technical Principles and Clinical Applications," *Acta Cardiologica Sinica*, vol. 32, no. 2, pp. 129–144, 2016. DOI: 10.6515/acs20150616a.

[15] A. Taylor and J. Bogaert, "Cardiovascular MR Imaging Planes and Segmentation," in *Clinical Cardiac MRI*, ser. Medical Radiology, J. Bogaert, S. Dymarkowski, A. Taylor, and V. Muthurangu, Eds., Berlin, Heidelberg: Springer, 2011. DOI: 10.1007/174_2011_333.

[16] B. D. Allen, N. S. Burris, P. J. Lombardi, and C. J. Francois, "Four-Dimensional Flow Magnetic Resonance Imaging in Cardiothoracic Imaging," *Advances in Clinical Radiology*, vol. 1, pp. 43–54, Sep. 2019. DOI: 10.1016/j.acra.2019.09.003.

[17] P. D. Gatehouse et al., "Applications of phase-contrast flow and velocity imaging in cardiovascular MRI," *European Radiology*, vol. 15, no. 10, pp. 2172–2184, 2005. DOI: 10.1007/s00330-005-2829-3.

[18] P. Dyverfeldt et al., "4D flow cardiovascular magnetic resonance consensus statement," *Journal of Cardiovascular Magnetic Resonance*, vol. 17, no. 1, p. 72, 2015. DOI: 10.1186/s12968-015-0174-x.

[19] K. S. Nayak et al., "Cardiovascular magnetic resonance phase contrast imaging," *Journal of Cardiovascular Magnetic Resonance*, vol. 17, no. 1, p. 71, 2015. DOI: 10.1186/s12968-015-0176-8.

[20] J. Lotz, C. Meier, A. Leppert, and M. Galanski, "Cardiovascular Flow Measurement with Phase-Contrast MR Imaging: Basic Facts and Implementation," *RadioGraphics*, vol. 22, no. 3, pp. 651–671, 2002. DOI: 10.1148/radiographics.22.3.g02ma11651.

[21] M. M. Bissell et al., "4d flow cardiovascular magnetic resonance consensus statement: 2023 update," *Journal of Cardiovascular Magnetic Resonance*, vol. 25, no. 1, p. 40, 2023, ISSN: 1097-6647. DOI: https://doi.org/10.1186/s12968-023-00942-z. [Online]. Available: https://www.sciencedirect.com/science/article/pii/S1097664723000406.

[22] S. Kozerke, J. Schwitter, E. M. Pedersen, and P. Boesiger, "Aortic and mitral regurgitation: Quantification using moving slice velocity mapping," *Journal of Magnetic Resonance Imaging*, vol. 14, no. 2, pp. 106–112, 2001. DOI: https://doi.org/10.1002/jmri.1159. eprint: https://onlinelibrary.wiley.com/doi/pdf/10.1002/jmri.1159. [Online]. Available: https://onlinelibrary.wiley.com/doi/abs/10.1002/jmri.1159.

[23] J. J. M. Westenberg et al., "Mitral valve and tricuspid valve blood flow: Accurate quantification with 3d velocity-encoded mr imaging with retrospective valve tracking," *Radiology*, vol. 249, no. 3, pp. 792–800, 2008, PMID: 18849503. DOI: 10.1148/radiol.2492080146. eprint: https://doi.org/10.1148/radiol.2492080146. [Online]. Available: https://doi.org/10.1148/radiol.2492080146.

[24] C. P. Blanken et al., "Quantification of mitral valve regurgitation from 4d flow mri using semiautomated flow tracking," *Radiology: Cardiothoracic Imaging*, vol. 2, no. 5, e200004, 2020, PMID: 33778618. DOI: 10.1148/ryct.2020200004. eprint: https://doi.org/10.1148/ryct.2020200004. [Online]. Available: https://doi.org/10.1148/ryct.2020200004.

[25] K. O'Shea and R. Nash, *An introduction to convolutional neural networks*, 2015. arXiv: 1511.08458 [cs.NE]. [Online]. Available: https://arxiv.org/abs/1511.08458.

[26] R. A. Gonzales, J. Lamy, F. Seemann, E. Heiberg, J. A. Onofrey, and D. C. Peters, "Tvnet: Automated time-resolved tracking of the tricuspid valve plane in MRI long-axis cine images with a dual-stage deep learning pipeline," in *Medical Image Computing and Computer Assisted Intervention – MICCAI 2021*, M. de Bruijne et al., Eds., Springer International Publishing, 2021, pp. 567–576. DOI: 10.1007/978-3-030-87231-1_55.

[27] R. A. Gonzales et al., "Mvnet: Automated time-resolved tracking of the mitral valve plane in cmr long-axis cine images with residual neural networks: A multicenter, multi-vendor study," *Journal of Cardiovascular Magnetic Resonance*, vol. 23, no. 1, pp. 1–15, 2021. DOI: 10.1186/s12968-021-00824-2.

[28] Medviso, *Medviso*, Accessed 2026-05-28, 2026. [Online]. Available: https://medviso.com/.

[29] F. Seemann, U. Pahlm, K. Steding-Ehrenborg, H. Arheden, and M. Carlsson, "Automated time-resolved tracking algorithm of the atrioventricular plane displacement in CMR images," *Journal of Cardiovascular Magnetic Resonance*, vol. 18, no. Suppl 1, P43, 2016. DOI: 10.1186/1532-429X-18-S1-P43.